pipette solution contained (mM): 70 potassium aspartate, 50 KCl, 10 KH_2PO_4, 1 $MgCl_2$, 3 Na_2-ATP, 0.1 Li_2-GTP, 5 EGTA, and 5 HEPES, and pH was adjusted to 7.2 with KOH. Liquid junctional potential between the test solution and the pipette solution was measured to be around −10 mV and was corrected. HMR1556 (a kind gift from Drs. H.J. Lang and J. Pünter, Aventis Pharma Deutschland GmbH) was added from 10 mM stock solution in DMSO to the external solution (final DMSO concentration did not exceed 0.01%).

To obtain the deactivation time constant, the time course of decaying tail current at −50 mV were fitted to a single exponential function:

$$I(t) = A + B\exp(-t/\tau),$$

where I(t) means the tail current amplitude at time t, A and B are constants, and τ is the deactivation time constant.

All data are presented as mean ± standard error of the mean (SEM). Statistical analysis was performed by analysis of variance (ANOVA) followed by Tukey-Kramer post hoc comparison. Statistical significance was set at $P < 0.05$.

Cell Preparation and Confocal Imaging

For the immunofluorescence study, we constructed a hemagglutinin (HA)-tagged *KCNE3* plasmid (wild type [WT] and mutant). An HA epitope (YPYDVPDYA) was introduced into the N-terminus of *KCNE3* cDNA, using an HA-tagged 5′ primer with a KpnI restriction site at the 5′ end and a 3′ primer with BsrGI at the 3′ end. The full-length cDNA fragment of human *KCNQ1* was subcloned into pCI-neo. COS7 cells were transfected with 1.0 &mug of HA-tagged pCR3.1-*KCNE3* (WT or mutant) and 1.0 &mug of pCI-neo-*KCNQ1* plasmid in 35-mm glass-bottom dishes, using Fugene6 (Roche Diagnostics, Basel, Switzerland) according to the manufacturer's instructions. At 48λhr later, the cells were washed twice with phosphate buffered saline (PBS), followed by incubation with a mouse anti-HA primary antibody (1:500) (Covance Research Products, Inc., Berkeley, CA) for 30λminutes at 37°C. The cells were then washed twice with PBS and incubated with an anti-mouse antibody conjugated to the Alexa 488 fluorophore (1:500) (Molecular Probes, Eugene, OR) as a secondary antibody for 30λminutes at 37°C. Finally, cells were washed with and immersed in Opti-Mem, and confocal images were obtained with a Zeiss LSM 510 (Carl Zeiss GmbH, Jena, Germany).

Results

Mutation Analysis

In 485 LQTS probands, we identified two novel missense mutations and one SNP in E3 (Figs. 1 and 2). The first mutation was a single nucleotide alternation (c.296G>A) (Fig. 1A) resulting in an amino acid substitution from an arginine at residue 99 with a histidine (p.R99λH). The second mutation was a single nucleotide change (c.10A>G) (Fig. 2A), causing an amino acid substitution p.T4A, replacing a threonine at residue 4 with an alanine. This T4A missense mutation was identified in two probands. Another proband was found to have a p.P39R polymorphism, which was reported as an SNP (rs34604640: C>G). These three variants were absent in 200 unrelated healthy individuals (400 alleles) from the general Japanese population. They are located in the N-terminus (T4A and P39R) and C-terminus (R99λH), respectively. We further searched for another mutation in LQTS-related genes in these probands carrying E3 mutations (see Materials and Methods). In one of the KCNE3-T4A carriers, we identified a *KCNH2*-p.G572S mutation and in the proband with the P39R polymorphism a *KCNH2*-p.W563G mutation. SNP c.198 T>C (rs2270676), which causes no amino acid substitution (p.F66F), was identified heterozygously in roughly 20% of both LQTS probands and healthy individuals.

Phenotypic Characterization

Patient 1

The novel mutation p.R99λH was found in a 76-year-old female suffering from drug-induced TdP. Her resting 12-lead electrocardiograph (ECG) before administration of disopyramide (Fig. 1B-a) displayed sinus rhythm with normal QTc (438 ms). Because of repeated paroxysmal AF, she was started on 300λmg of disopyramide per day. At 10 days after disopyramide intake, her level of consciousness decreased and ECGs displayed frequent premature ventricular contractions (PVCs) and TdP (Fig. 1B-b). Her heart rate was 66 beats per minute (bpm), and her QTc time was prolonged to 580 ms. Serum K level was within normal range (4.0 mEq/L). Disopyramide was immediately stopped, and temporary pacing was immediately started at 90 bpm. In 3 days, TdP attacks ceased and QTc intervals returned within normal range. She had no family history of sudden cardiac death and LQTS. We did not conduct genetic analyses on the relatives of this patient, due to a lack of consent.

Patient 2

A p.T4A mutation was identified in a 16-year-old boy who had QT prolongation discovered during his school's annual health checkup. He had no history of faintness or syncope and no family history of syncope or sudden death. His resting ECG (Fig. 2B) revealed bradycardia for age (48 bpm) and QT prolongation (QTc = 525 ms). Genetic analysis on other LQTS-related genes revealed a *KCNH2*-G572S missense mutation which had been previously reported [Tester et al., 2005]. His mother and sister also remained asymptomatic but had the same heterozygous set of genetic variants (E3-T4A and *KCNH2*-G572S). Their ECGs also displayed the prolongation of QTc intervals: 520 ms and 560 ms (data not shown).

Patient 3

A p.T4A mutation was also identified in another unrelated proband, a 68-year-old female, who experienced hypokalemia-induced TdP at age 60 years. After correction of serum potassium levels, her QTc time was normalized to 430 msec (Fig. 2C). Two years after the TdP event, she was diagnosed with cardiac sarcoidosis and was started on steroid hormone therapy. Though her daughter also carried the E3-T4A mutation, she was asymptomatic with borderline QTc.

Patient 4

A p.P39R amino acid substitution was identified in a 32-year-old female who was also identified to have a novel *KCNH2* missense mutation, p.W563G. She experienced repeated episodes of late night syncope at ages 15, 21, and 26 years. Figure 3 displays her 12-lead ECG demonstrating marked QT prolongation (QTc = 512 msec) and notched T waves, suggesting LQTS type

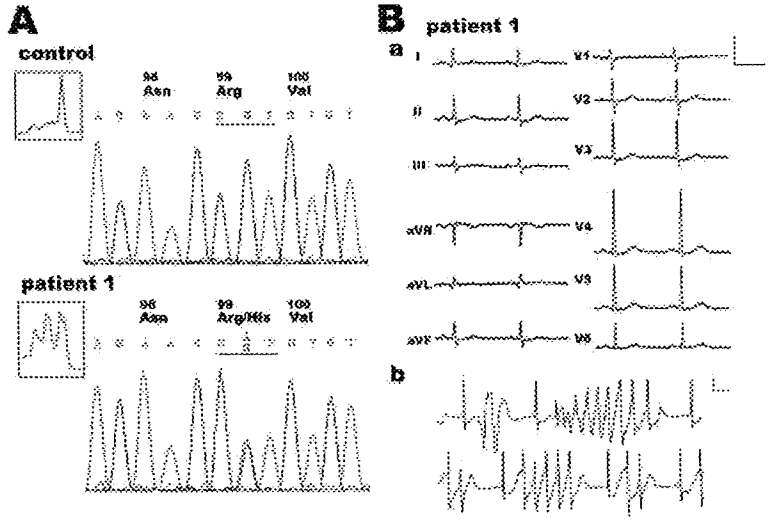

Figure 1. Molecular discovery and clinical characterization of R99H-KCNE3. **A:** DHPLC (insets) and DNA sequence analyses of normal control and Patient 1. DNA sequencing chromatograms demonstrate an arginine (Arg) to histidine (His) substitution at residue 99. **B:** ECGs of Patient 1. (a) 12-lead ECG and (b) monitoring ECG of TdP in a 76-year-old female patient. Scale bars indicate 1 mV and 400 ms. [Color figure can be viewed in the online issue, which is available at www.interscience.wiley.com.]

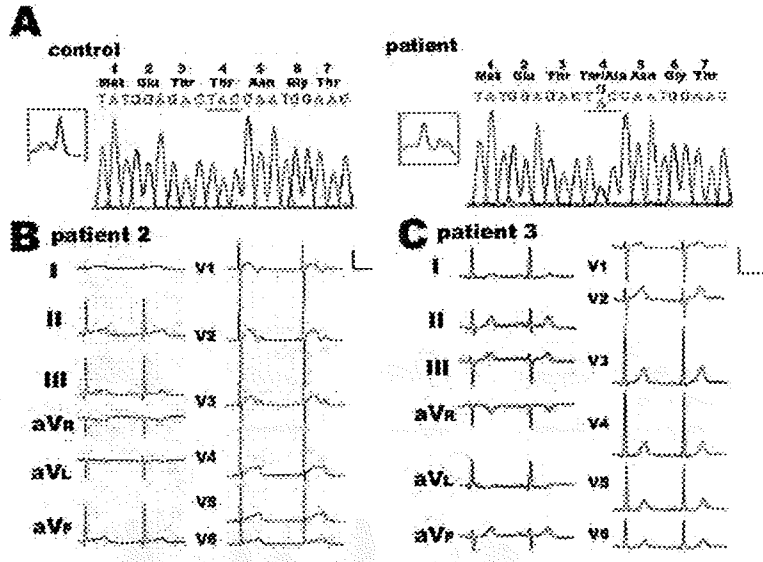

Figure 2. Molecular discovery and clinical characterization of T4A-KCNE3. **A:** DHPLC (insets) and DNA sequence analysis of normal control and patient. DNA sequencing chromatograms demonstrate a threonine (Thr) to alanine (Ala) substitution at residue 4. **B:** The 12-lead ECG of Patient 2. **C:** The 12-lead ECG of Patient 3. [Color figure can be viewed in the online issue, which is available at www.interscience.wiley.com.]

2. E3-P39R was reported as an SNP (rs34604640: C>G); however, P39R was absent in 400 control alleles from healthy Japanese cohorts. Therefore, we conducted a functional analysis of three mutants including P39R.

Biophysical Properties of KCNQ1 Channels Coexpressed With KCNE3

To clarify the functional consequences of these missense mutations (R99λH, T4A, and P39R) on E3, we assessed the biophysical properties of the mutated E3 clone by using the stably expressing human KCNQ1-CHO cell line. Figure 4A shows representative examples of whole-cell currents recorded from CHO cells stably expressing the Q1 channel transfected with or without E3 (WT or mutant). Insets to the right of each recording illustrate expanded views of the tail current elicited after return to −50 mV from test potentials. The current amplitudes were normalized by cell capacitances (current densities). Recordings from cells expressing the Q1 channel alone (left panel of Fig. 4A) displayed small amplitudes of time-dependent outward currents during depolarizing test potentials, followed by slowly deactivating tail currents on return to −50 mV. In contrast, transfection of stable Q1 cells with E3-WT (second panel in Fig. 4A) gave rise to large amplitudes of currents composed of at least two components: 1) a time-dependent outward current activated during depolarizing steps; and 2) a constitutively active background

current during depolarizing and hyperpolarizing (−50 mV) steps, as previously reported [Bendahhou et al., 2005; Schroeder et al., 2000]. After the recordings of Q1 with or without E3 current, we applied HMR1556 (1 &muM), a selective Q1 channel blocker. Though the sensitivity on the Q1 alone and Q1+E3 channel of chromanol 293B, another Q1 channel blocker, was different [Bett et al., 2006], both Q1 and Q1+E3 currents were almost totally abolished by only 1 &muM HMR1556 (lower panels of Fig. 4A).

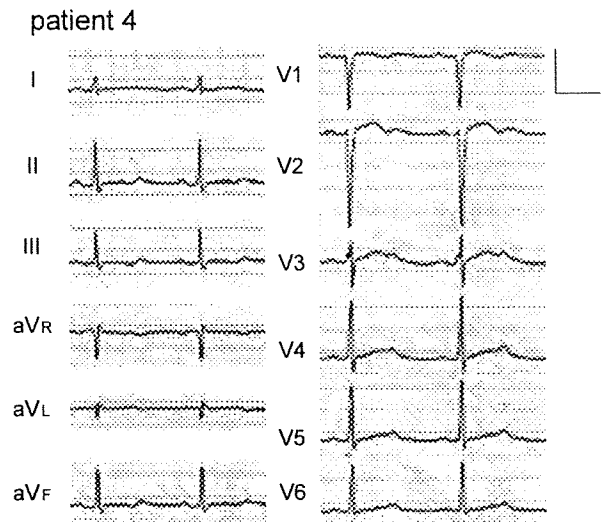

Figure 3. The 12-lead ECG of Patient 4 with QT prolongation. The patient was found to have a KCNE3-SNP, P39R, and a KCNH2-mutation, W536G.

HMR1556-sensitive current densities at the end of test pulse (Fig. 4B) were averaged from data and are plotted as the function of test voltage of Q1 (closed square), Q1+E3-WT (closed circle), Q1+E3-R99λH (open triangle), Q1+E3-T4A (open circle), and Q1+E3-P39R (closed triangle). Currents reconstituted by Q1 alone were activated at potentials greater than −40 mV, whereas those by Q1+E3 (WT and all mutants) were active at all test potentials and exhibited a strong outward rectification with a reversal potential close to E_K (−84 mV as predicted by Nernst equation). All three E3 mutants, E3-R99λH, E3-T4A, and E3-P39R, produced membrane currents with properties qualitatively similar to those of E3-WT. As summarized in Figure 4C, the current densities for the Q1+E3-R99λH current at +40 and −120 mV were 163.7±26.3 and −10.1±2.6 pA/pF, respectively. These values were significantly smaller than those of the Q1+E3-WT (301.6±33.3 pA/pF at +40 mV and −24.5±4.2 pA/pF at −120 mV, $P<0.05$). Q1+E3-T4A and Q1+E3-P39R displayed no statistically significant difference. The deactivation time constant for tail currents was significantly decreased by coexpression of E3 with Q1, but these three mutations in E3 had no significant effect on deactivation kinetics (Fig. 4D).

Cellular Immunocytochemistry of KCNE3

It was reported that no E3 could be expressed on the plasma membrane in the absence of Q1 [Schroeder et al., 2000]. This was reconfirmed in our experimental protocol; the two left columns in Figure 5 show that HA-tagged E3 is not detected by Alexa 488 conjugated HA antibodies in nonpermeabilized COS7 cells in the

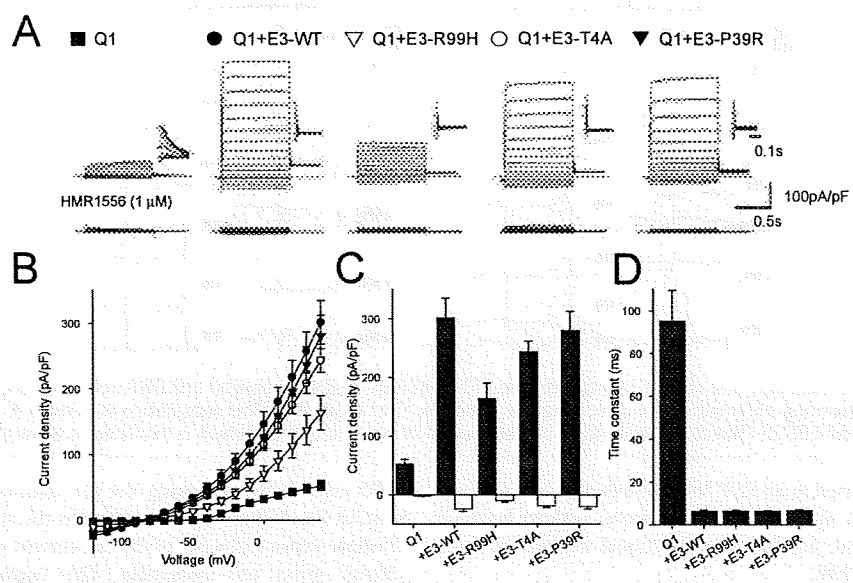

Figure 4. Functional analysis of KCNE3 and its mutants in a CHO cell line stably expressing KCNQ1 channel. **A:** Whole-cell membrane currents recorded from stable KCNQ1-CHO cells transfected without (Q1) or with KCNE3-wild type (Q1+E3-WT), KCNE3-R99λH (Q1+E3-R99λH), KCNE3-T4A (Q1+E3-T4A), or KCNE3-P39R (Q1+E3-P39R). Cells were held at −80 mV and stepped to various test potentials ranging from −120 to +40 mV in 10 mV steps for 1 sec before (upper panel) and during (lower panel) exposure to HMR1556 (1 μM). Dotted line indicates zero current level. Scale bars indicate 0.5 sec and 100 pA/pF. Insets to right of each recording illustrate expanded views of tail current elicited after return to −50 mV from test potentials. Scale bar indicates 0.1 sec. **B:** Current-voltage relationships for mean values of HMR1556-sensitive currents measured at the end of test pulses in CHO cells expressing Q1 (closed square, n = 5), Q1+E3-WT (closed circle, n = 14), Q1+E3-R99λH (open triangle, n = 12), Q1+E3-T4A (open circle, n = 12), or Q1+E3-P39R (closed triangle, n = 10). **C:** Summary of the current density measured at +40 (black bar) and −120 mV (white bar). Columns and error bars indicate mean±SEM. **D:** Deactivation time constant calculated by fitting a single exponential function to tail current at −50 mV after depolarization to +40 mV.

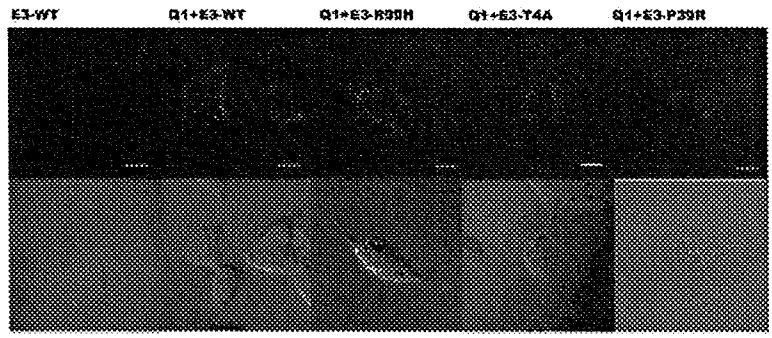

Figure 5. Cell surface expression of WT and mutant KCNE3 channels in nonpermeabilized cell. Upper panels of each column indicate HA-tagged KCNE3 (E3) (WT and three variants) with Alexa 488-conjugated antibodies with or without KCNQ1. Lower panels show merge of green fluorescence and light transmission images. Scale bars indicate 50 &mum in E3-WT and 10 &mum in others.

absence of Q1 cotransfection. In contrast, HA-tagged E3 could be visualized in the presence of Q1, which indicates that the Q1 protein is necessary for E3 to be successfully trafficked to the cell membrane. Q1 plus HA-tagged E3 channels generated currents similar to those of Q1 plus untagged E3 channels (data not shown). Figure 5 illustrates representative sets of confocal images. COS7 cells were transfected with tagged E3 (WT, T4A, and R99λH) and Q1. All Q1 plus HA-tagged E3 exhibited green fluorescence in the plasma membrane indicating that these channels were trafficked to the plasma membrane normally.

Discussion

In the present study, we report three E3 variants found in 485 LQTS probands. One of the two novel mutations, R99λH, displayed a significant decrease in outward currents when coexpressed with Q1. The proband with the E3-R99λH mutation suffered from drug-induced TdP. After washout of disopyramide, her QTc time on the ECG returned within normal range. The drug probably induced remarkable QT prolongation and TdP in the presence of a reduced repolarization reserve [Roden, 1998], which was associated with the E3-R99λH mutation.

The expression of E3 was confirmed in the human heart [Bendahhou et al., 2005; Lundquist et al., 2005, 2006]. Though neither the presence nor potential function of Q1+E3 channels in human cardiac myocytes have been determined, E3 conformed a functional channel in interaction with Q1, constitutively open potassium channel [Schroeder et al., 2000]. In addition, azimilide-sensitive Q1+E3 like currents were recorded in canine myocytes [Dun and Boyden, 2005]. On account of these results, E3 is assumed to have a physiological role in human heart. Mazhari et al. [2002] studied the effects of E3 on action potential duration (APD) in in vivo transduction of guinea pig ventricular myocytes. APD of E3-transduced myocytes was significantly reduced compared to that of control myocytes. Under the assumption that E3 might interact with KCNH2, they also performed a series of tests using an I_{Kr} blocker (E-4031) to determine whether the APD shortening was due to the interaction with E3 and KCNH2. However, E-4031 did not affect the APD in E3-transduced myocytes. As a result, the APD shortening appeared to be a result of the interaction between Q1 and E3. Although ventricular myocytes are repolarized mainly by Q1+E1 (I_{Ks}) and KCNH2 (I_{Kr}) in human hearts, we believe that the mutant E3 could prolong APD through interaction with Q1. We recently reported the knockdown of E3 expression using RNA interference in guinea pig ventricular myocytes [Toyoda et al., 2008]. The knockdown of E3 was found to prolong the APD, suggesting that E3 may play a physiological role in repolarization of cardiac action potential.

The interaction between KCNH2 and E3 is not established yet. In the experiments using *Xenopus* oocytes, KCNH2 currents were suppressed by coinjection with E3 [Schroeder et al., 2000]. On the contrary, the interaction in horse hearts could not be displayed by means of sequential immunoprecipitation and immunoblotting [Finley et al., 2002]. In addition, the I_{Kr} blocker did not affect APD in E3-transduced myocytes in guinea pigs [Mazhari et al., 2002]. Consequently, we supposed that KCNH2 plus E3 channel would affect very little for repolarization. We therefore did not pursue further examination on the interaction with KCNH2 and E3 using mammalian cell lines.

Regarding the E3-T4A mutation, we postulated that the E3-T4A has minor effects on the QT prolongation, based on the fact that no E3-T4A variant was found in our normal control. Though one of the probands had a *KCNH2*-G572S mutation [Tester et al., 2005] which is supposed to be the major reason for the QT prolongation, another proband had no mutation in major LQTS-related genes. In our biophysical assay, the mutant caused no significant difference in Q1+E3-T4A channel currents; therefore we could not display the association between E3-T4A mutation and QT prolongation. In patient 3, hypokalemia triggered the TdP, accordingly reducing extracellular potassium level may affect the currents through Q1+E3-T4A channels. Or E3 may also interact with another potassium channel alpha-subunit that affects the repolarization of cardiac myocytes, and the E3-T4A mutation may decrease the outward current to prolong QT time. We have to take into account that E3-T4A is a rare SNP, because the correlation between phenotype and genotype in our patients was not common and the number of our control was smaller compared to the studied cases.

E3-P39R may also have functional effects on repolarization. However, our proband with E3-P39R had a compound *KCNH2*-W563G mutation, as well as typical symptoms and ECG findings (Fig. 3) compatible with type 2 LQTS. In addition, functional analysis of the Q1+E3-P39R channel displayed smaller current densities than those of the Q1+E3-WT channel; however there was no statistical difference. Therefore we considered E3-P39R as a rare normal variant in Japanese.

Concerning another α subunit which interacts with KCNE3, Kv4.3 potassium channel encoded by *KCND3* produces transient outward potassium conductance (I_{to}) in the heart and KCNE3 inhibits the Kv4.3 currents [Lundby and Olesen, 2006; Radicke et al., 2006], even in the presence of KChIP2. Hence, there is a possibility that our E3 mutants affect the Kv4.3 current and prolong QT interval.

In conclusion, we identified three E3 variants among 485 Japanese LQTS probands, and one of which significantly reduced currents by interacting with Q1. Though the proband had remained asymptomatic in the absence of risk predisposing to QT prolongation, she fell into highly critical condition by taking disopyramide for AF at age of 76. Therefore, identification of E3 mutations with possible phenotypic effects provides us with information for our understanding of the mechanism of LQTS.

Acknowledgments

We thank the Japanese LQT families for their willingness to participate in this study. We are grateful to Ms. Arisa Ikeda for providing expert technical assistance, and we thank Dr. Takahiro Mitsueda for phenotypic data collection and Mr. Richard Kaszynski for reading the manuscript. W.S., Y.M., and M.H. were supported by a Health Sciences Research grant (H18-Research on Human Genome-002) from the Ministry of Health, Labour and Welfare, Japan.

References

Abbott GW, Sesti F, Splawski I, Buck ME, Lehmann MH, Timothy KW, Keating MT, Goldstein SA. 1999. MiRP1 forms I_{Kr} potassium channels with HERG and is associated with cardiac arrhythmia. Cell 97:175–187.

Abbott GW, Butler MH, Bendahhou S, Dalakas MC, Ptacek LJ, Goldstein SA. 2001. MiRP2 forms potassium channels in skeletal muscle with Kv3.4 and is associated with periodic paralysis. Cell 104:217–231.

Bendahhou S, Marionneau C, Haurogne K, Larroque MM, Derand R, Szuts V, Escande D, Demolombe S, Barhanin J. 2005. In vitro molecular interactions and distribution of KCNE family with KCNQ1 in the human heart. Cardiovasc Res 67:529–538.

Bett GC, Morales MJ, Beahm DL, Duffey ME, Rasmusson RL. 2006. Ancillary subunits and stimulation frequency determine the potency of chromanol 293B block of the KCNQ1 potassium channel. J Physiol 576(Pt 3):755–767.

Dun W, Boyden PA. 2005. Diverse phenotypes of outward currents in cells that have survived in the 5-day-infarcted heart. Am J Physiol Heart Circ Physiol 289:H667–H673.

Finley MR, Li Y, Hua F, Lillich J, Mitchell KE, Ganta S, Gilmour RF, Jr, Freeman LC. 2002. Expression and coassociation of ERG1, KCNQ1, and KCNE1 potassium channel proteins in horse heart. Am J Physiol Heart Circ Physiol 283:H126–H138.

Lundby A, Olesen SP. 2006. KCNE3 is an inhibitory subunit of the Kv4.3 potassium channel. Biochem Biophys Res Commun 346:958–967.

Lundby A, Ravn LS, Svendsen JH, Hauns S, Olesen SP, Schmitt N. 2008. KCNE3 mutation V17λM identified in a patient with lone atrial fibrillation. Cell Physiol Biochem 21:47–54.

Lundquist AL, Manderfield LJ, Vanoye CG, Rogers CS, Donahue BS, Chang PA, Drinkwater DC, Murray KT, George AL, Jr. 2005. Expression of multiple KCNE genes in human heart may enable variable modulation of I_{Ks}. J Mol Cell Cardiol 38:277–287.

Lundquist AL, Turner CL, Ballester LY, George AL, Jr. 2006. Expression and transcriptional control of human KCNE genes. Genomics 87:119–128.

Mazhari R, Nuss HB, Armoundas AA, Winslow RL, Marban E. 2002. Ectopic expression of KCNE3 accelerates cardiac repolarization and abbreviates the QT interval. J Clin Invest 109:1083–1090.

Morin TJ, Kobertz WR. 2007. A derivatized scorpion toxin reveals the functional output of heteromeric KCNQ1-KCNE K^+ channel complexes. ACS Chem Biol 2:469–473.

Moss AJ, Kass RS. 2005. Long QT syndrome: from channels to cardiac arrhythmias. J Clin Invest 115:2018–2024.

Ohno S, Zankov DP, Yoshida H, Tsuji K, Makiyama T, Itoh H, Akao M, Hancox JC, Kita T, Horie M. 2007. N- and C-terminal KCNE1 mutations cause distinct phenotypes of long QT syndrome. Heart Rhythm 4:332–340.

Radicke S, Cotella D, Graf EM, Banse U, Jost N, Varro A, Tseng GN, Ravens U, Wettwer E. 2006. Functional modulation of the transient outward current Ito by KCNE beta-subunits and regional distribution in human non-failing and failing hearts. Cardiovasc Res 71:695–703.

Roden DM. 1998. Taking the "idio" out of "idiosyncratic": predicting torsades de pointes. Pacing Clin Electrophysiol 21:1029–1034.

Schroeder BC, Waldegger S, Fehr S, Bleich M, Warth R, Greger R, Jentsch TJ. 2000. A constitutively open potassium channel formed by KCNQ1 and KCNE3. Nature 403:196–199.

Tester DJ, Will ML, Haglund CM, Ackerman MJ. 2005. Compendium of cardiac channel mutations in 541 consecutive unrelated patients referred for long QT syndrome genetic testing. Heart Rhythm 2:507–517.

Toyoda F, Ueyama H, Ding WG, Matsuura H. 2006. Modulation of functional properties of KCNQ1 channel by association of KCNE1 and KCNE2. Biochem Biophys Res Commun 344:814–820.

Toyoda F, Zankov DP, Ding WG, Matsuura H. 2008. Functional regulation of cardiac KCNQ1 potassium channel by association of KCNE3. [Abstract]. 2008 Biophysics Society Meeting Abstracts, February 2–6, 2008. Biophys J 94(Suppl):3025.

Circ J 2009; 73: 810–817

Phenotypic Overlap of Cardiac Sodium Channelopathies

Individual-Specific or Mutation-Specific?

Naomasa Makita, MD

Mutations in the cardiac sodium channel gene *SCN5A* are responsible for a spectrum of hereditary arrhythmias, including type-3 long QT syndrome (LQT3), Brugada syndrome (BrS), conduction disturbance and sinus node dysfunction. These syndromes were originally regarded as independent entities with distinct clinical manifestations and biophysical properties, but recent evidence shows considerable clinical overlap, implying a new disease entity known as an overlap syndrome of cardiac sodium channelopathy. Class IC sodium-channel blockers often induced the BrS phenotype in some patients with LQT3, confirming the clinical overlap of LQT3 and BrS. It also raises a concern about the safety of the class IC drug and questions about the determinants of overlap. Here, an overview is given of current knowledge on the clinical features, prevalence, and molecular and biophysical mechanisms underlying overlap syndrome to gain more insight into this complex issue and generate better therapeutic strategies for patient management. (*Circ J* 2009; 73: 810–817)

Key Words: Brugada syndrome; Flecainide; Long QT syndrome; Overlap syndrome; *SCN5A*

Structure–Function of Cardiac Sodium Channels

The voltage-gated sodium (Na) channel is responsible for the rapid upstroke of the action potential in most of the excitable tissues, and plays a pivotal role in the initiation, propagation, and maintenance of normal cardiac rhythm. The cardiac Na channel comprises the most prevalent pore-forming α-subunit (Nav1.5) encoded by the gene *SCN5A* located on chromosome 3p21 and auxiliary β subunits (Nav β1–Nav β4) encoded by the genes *SCN1B–SCN4B*, respectively. The α-subunits have a 4-fold symmetry macromolecule consisting of structurally homologous domains (D1–D4) each containing 6 membrane-spanning segments (S1–S6) and a region (S5–S6 loop) controlling ion selectivity and permeation. The positively charged S4 segment of each domain functions as a voltage sensor.[1,2]

The Na channels switch between 3 functional states (closed, open, inactivated), depending on the membrane potential. Membrane depolarization causes a rapid rise in local Na permeability because of opening (activation) of the Na channels from their resting closed state. Normally, activation of the Na channels is transient, because of inactivation, another gating process mediated by structures located on the cytoplasmic face of the channel protein (mainly the D3–D4 linker). The Na channels cannot reopen until the membrane is repolarized and they recover from inactivation. Membrane repolarization is achieved by fast inactivation of the Na channels and is augmented by activation of voltage-gated K channels. Activation, inactivation, and recovery from inactivation occur within a few milliseconds. In addition to these rapid gating transitions, the Na channels are also susceptible to slower inactivating processes (slow inactivation) if the membrane remains depolarized for a longer time. These slower events may contribute to the availability of active channels under various physiological conditions.

(Received January 6, 2009; revised manuscript received January 26, 2009; accepted January 27, 2009; released online March 31, 2009)
Department of Cardiovascular Medicine, Hokkaido University Graduate School of Medicine, Sapporo, Japan
Mailing address: Naomasa Makita, MD, Department of Cardiovascular Medicine, Hokkaido University Graduate School of Medicine, Kita-15, Nishi-7, Kita-ku, Sapporo 060-8638, Japan. E-mail: makita0310@yahoo.co.jp

Genetics of Cardiac Sodium Channelopathies

Mutations of *SCN5A* are responsible for a spectrum of hereditary arrhythmias, including type-3 congenital long QT syndrome (LQTS; LQT3),[3,4] acquired LQTS,[5] Brugada syndrome (BrS; BrS1),[5,6] cardiac conduction disturbance (CCD),[7] congenital sick sinus syndrome (SSS),[8] atrial standstill,[9–11] AV block,[12] sudden infant death syndrome,[13–15] and familial atrial fibrillation[16–18] (**Table 1**). In addition to these primary electrical diseases, which usually do not have structural abnormalities, *SCN5A* mutations have also been reported in patients with dilated cardiomyopathy.[16,19] Moreover, recent genetic studies have indicated that mutations

Table 1. Inherited Cardiac Sodium Channelopathies

1. Cardiac Na channel α-subunit (*SCN5A*)
Congenital long QT syndrome (LQT3)
Acquired long QT syndrome
Brugada syndrome (BrS1)
Cardiac conduction disturbance (CCD)
Congenital sick sinus syndrome (SSS1)
Atrial standstill
AV block
Sudden infant death syndrome (SIDS)
Familial atrial fibrillation (FAF)
Dilated cardiomyopathy (DCM)
2. Sodium channel β1-subunit (*SCN1B*)
Brugada syndrome with CCD (BrS5)
3. Sodium channel β4-subunit (*SCN4B*)
Congenital long QT syndrome (LQT10)

Table 2. Mutations in Overlapping Cardiac Sodium Channelopathies

Clinical manifestation	*SCN5A* and *SCN1B* (*) mutations	References
BrS+LQT3 (±CCD)	V411M, D1114N, W1193X, T1350T, ΔK1500, ΔKPQ, R1623P, P3006A	22, 35, 37, 42–46
BrS+LQT3+SSS (±CCD)	G1382S, ΔF1617, E1784K, 1795insD	8, 32, 33, 35, 40, 41, 47, 48
BrS+SSS	E161K, T187I, E1225K, ΔK1479, K1578fs, R1623X	31, 49, 50
BrS+AS	R367H	11
BrS+CCD	P336L, D356N, R376H, N406S, G752R, F861fs953X, E867X, G1319V	50–54
	G1406R, I1660V, S1710L, S1812X, E87Q*, Y179X*	20, 30, 50, 51, 55–57
DCM (+/− CCD+SSS+AF)	T220I, R814W, F851fs, D1275N, D1595H	9, 16, 19
CCD+SSS/AS	G1408R	8
AS+AF	L312P	10
LQT3+CCD	P1332L, V1763M, M1766L, V1777M, P2005A	58–65

BrS, Brugada syndrome; LQT3, type-3 long QT syndrome; SSS, sick sinus syndrome; CCD, cardiac conduction disturbance; AS, atrial standstill; DCM, dilated cardiomyopathy; AF, atrial fibrillation.

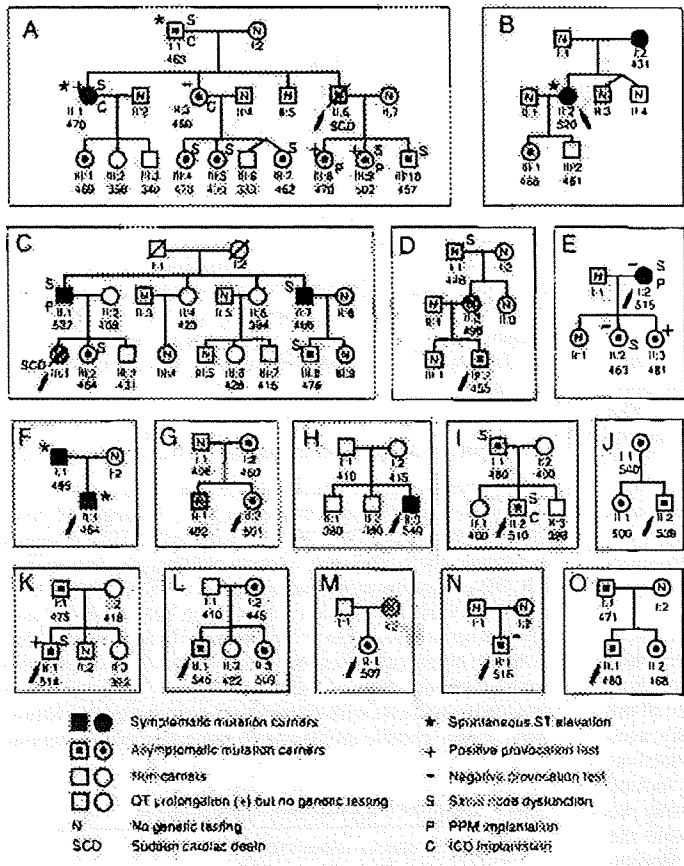

Figure 1. Pedigrees of 15 LQT3 families (A–O) carrying E1784K are shown. Probands are indicated by an arrow. 10 symptomatic mutation carriers, shown by the filled symbols, had episodes of syncope (n=9) and unexplained palpitations (n=1, B, II:2). Asymptomatic mutation carriers (n=31) are shown as symbols with a dot, and shaded symbols are the individuals with QT prolongation who declined genetic testing or sudden cardiac death victims (SCD; A, II:6 and C, III:1). *Individuals exhibiting ST elevation in the right precordial leads. Values for QTc intervals are given beneath each symbol. The Na-channel provocation test was positive in individuals with + (A, II:1, A, III:8, A, III:9; E, II:3, K, II:1), and negative in the individuals with − (A, II:3; E, I:2, E, II:2, N, II:1). Individuals with a positive and negative Na-channel blocker provocation test are shown as + and −, respectively. (Modified with permission from Makita et al. *J Clin Invest* 2008; 118: 2219–2229[31])

in the Na channel β-subunit genes, *SCN1B* and *SCN4B*, are associated with type-5 BrS complicated with CCD (BrS5)[20] and type-10 LQTS (LQT10), respectively.

Biophysical Properties of Cardiac Sodium Channelopathies

Congenital LQTS is characterized by prolongation of the QT interval on surface ECGs and an increased risk of potentially fatal ventricular arrhythmias,especially torsade de pointes?[1] The QT interval is determined by the cardiac action potential, which is orchestrated by a fine balance between inward and outward currents expressed in myocardial cells. After the first identification in 1995 of the *SCN5A* mutation ΔKPQ, comprising a deletion of 3 conserved amino acids, 1505–1507, in the cytoplasmic D3–D4 linker,[32] more than 100 distinct *SCN5A* mutations responsible for LQT3 have been reported. The common in vitro consequence of most of these mutations is a persistent Na current during the action potential plateau because of destabilized fast Na channel inactivation.[3] This failure of fast inactivation shifts the ionic balance during the plateau phase toward the

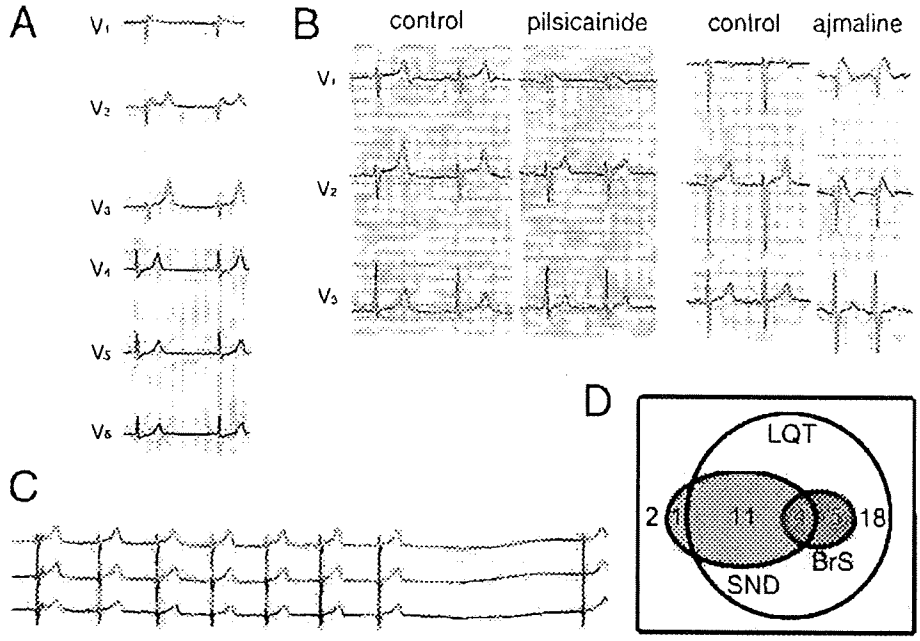

Figure 2. ECG characteristics of E1784K mutation carriers. QT prolongation (QTc = 470 ms) and spontaneous saddleback type ST elevation observed in the right precordial leads in a carrier (Figure 1A, II 1). (A) ECG recordings before and after the Na-channel blocker provocation test. Pilsicainide (Left, patient K, II:1) induced a coved-type ST elevation in V1 and the QTc was concomitantly shortened (QTc: control 495 ms, pilsicainide 459 ms). Ajmaline (Right, patient A, III:9) also induced a coved-type ST elevation in V1 and V2 and QTc shortening (control 501 ms, ajmaline 490 ms). (B) SND demonstrated by a 3.9 s sinus arrest in a carrier (A, I:1). (C) Venn diagram representing electrophysiological manifestation of 41 *SCN5A*-E1784K mutation carriers: 38 carriers had an abnormally long QTc; 3 individuals had a normal QTc, and 1 exhibited sinus node dysfunction (SND) only. SND and Brugada syndrome were observed in 15 and 9 individuals, respectively, with 4 displaying both phenotypes. (Modified with permission from Makita et al. *J Clin Invest* 2008; 118: 2219–2229[41])

inward current (gain-of-function) and delays repolarization, thus increasing the action potential duration and the corresponding QT interval. Na channel blockers, such as mexiletine (class IB) or flecainide (class IC), shorten the QT in patients with LQT3 by blocking of this persistent current;[23–25] therefore are theoretically useful in the management of affected patients.

BrS is another primary electrical disorder without underlying structural heart diseases characterized by the coved-type ST elevation in the right precordial leads.[26,27] It predisposes affected individuals to ventricular fibrillation (VF). Mutations in *SCN5A* are identified in 20–30% patients with BrS, and most of the heterologously expressed mutant Na channels exhibit biophysical abnormalities resulting in reduced cardiac Na current (loss-of-function).[28] Reduced Na current is thought to exaggerate differences in the action potential duration between the inner (endocardium) and outer (epicardium) layers of ventricular muscle, thereby favoring substrate promoting reentrant arrhythmias. Loss-of-function of the cardiac Na channels is either owing to (1) haplo-insufficiency because of non-functional mutations, (2) impaired altered channel-gating properties, including enhanced inactivation, disruption of activation and impaired recovery from inactivation, or (3) impaired intracellular trafficking and decreased membrane surface expression of the channel molecules.

Clinical Overlap of Cardiac Sodium Channelopathies

SCN5A mutations with loss-of-function properties have also been identified in patients with CCD,[7,29] SSS,[9] and atrial standstill,[9] and numbers of reports have shown that the mutation carriers tend to exhibit overlapping clinical properties of these syndromes[30,31] (**Table 2**). Importantly, such loss-of-function properties are apparently opposite to those described in LQT3 (gain-of-function), and different *SCN5A* mutations were initially linked to separate arrhythmias syndromes. Surprisingly, some LQT3 patients display ECG findings characteristic of BrS, suggesting that a single mutation can be associated with a wide spectrum of disease phenotypes. Such phenotypic overlap between LQT3 and BrS was first reported in a large multigenerational Dutch family with an insertion mutation 1795insD, in which the mutation carriers showed ECG features of both LQT3 and BrS, and sinus node dysfunction (SND).[32,33] Importantly, Na channel block in the overlap phenotype shortens QT, but exacerbated the ST segment elevation BrS phenotype, and thus enhances arrhythmia risk.[33] Biophysical studies demonstrated that the mutant channels displayed enhancement of both closed-state inactivation and slow inactivation, which was thought to sensitize carriers to the BrS phenotype during flecainide therapy,[34] in addition to the persistent Na current, a hallmark Na channel property of LQT3.

The overlap between the LQT3 and BrS phenotypes was also reported in other *SCN5A* mutations such as ΔKPQ,[35,36]

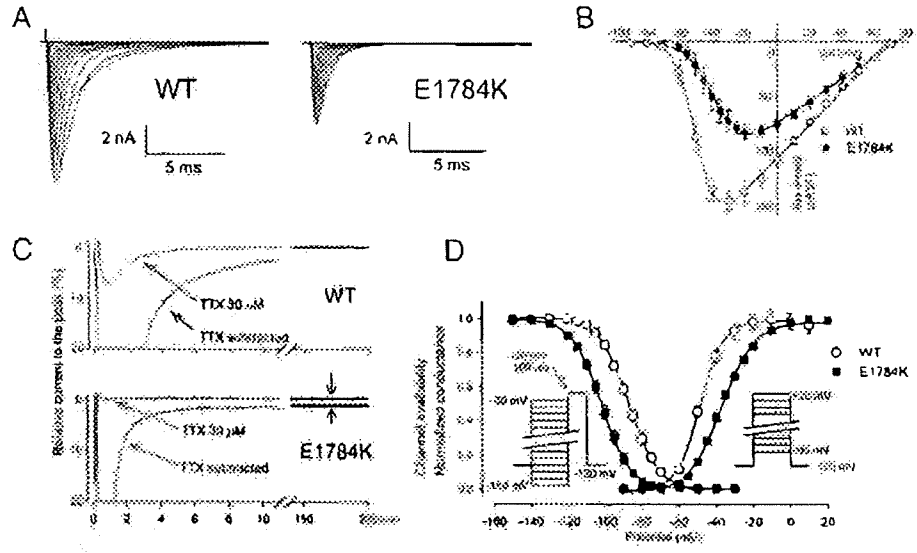

Figure 3. Properties of E1784K whole-cell current. (A) Representative whole-cell current traces obtained from tsA-201 cells transfected with either wild-type (WT) or E1784K Na channels, all studies were conducted in cells co-transfected with human sodium channel β1-subunits. Currents were recorded from a holding potential of −120 mV and stepped from −90 mV to +90 mV for 20 ms in 10 mV increments. (B) Current-voltage relationship. Current was normalized to cell capacitance to give a measure of Na current density. (C) Na currents were recorded with a test pulse potential of −20 mV from a holding potential of −120 mV showed prominent tetrodotoxin-sensitive late Na current (shown with arrows) and the faster decay in E1784K. (D) Steady-state availability for fast inactivation and the conductance-voltage relationship were measured with standard pulse protocols shown in the inset. Curves were fit with the Boltzmann equation. The voltage-dependence of steady-state fast inactivation and activation were significantly shifted in the hyperpolarizing (−15.0 mV) and depolarizing (+12.5 mV) directions, respectively. (Modified with permission from Makita et al *J Clin Invest* 2008; 118: 2219–2229[11])

E1784K[35] and ΔK1500[37] Prion et al showed the additional evidence for the elusive link between these 2 clinical syndromes by the fact that the class IC sodium channel blocker flecainide induced ST-segment elevation in the right precordial leads not only in patients with BrS, but also with LQT3[35] Of 13 patients in 7 LQT3 families (*SCN5A* mutations of V411M, T1304M, ΔK1500, ΔKPQ, R1626P, E1784K, P2006A), 6 showed flecainide-induced ST elevation. However, they failed to identify the determinants of flecainide-induced ST elevation in patients with LQT3. In fact, they assumed that the clinical overlap appeared to be individual-specific, rather than gene-specific or mutation-specific, most likely because the size of their patients was rather small. Nonetheless, these observations raise a concern about the safety of class IC drug therapy in LQT3 patients and questions about the underlying mechanisms.

Phenotypic variability in LQT3 has thus far been reported sporadically or only within a single kindred[32,33] Therefore, it is unclear whether development of the BrS phenotype in a patient with LQT3 is solely determined by the biophysical properties of the mutant channel, or by co-inherited genetic variations, gender, ethnicity, or other environmental factors. One approach to dissecting such phenotypic variability is to perform a clinical assessment of individuals with multiple pedigrees from genetically heterogeneous populations with the same mutation.

Clinical Phenotypes in 15 LQT3 Families With SCN5A-E1784K

From 7 institutions in Japan, Italy, Germany, UK and the US, 44 genotyped LQT3 families with different ethnic backgrounds were enrolled (Asian 20, Caucasian 24). E1784K was the most prevalent *SCN5A* mutation, identified in 15 families (34%). Two probands died suddenly, and 66 of the 93 surviving members underwent genetic testing. There were 41 mutation carriers and 25 non-carriers, and QTc was significantly prolonged in the carriers.

Spontaneous ST elevation in the right precordial leads occurred in 5/41 mutation carriers (Figure 1; coved-type: n=1, saddle-back type: n=4, Figure 2A). Nine mutation carriers without diagnostic ST elevation at baseline underwent provocation with flecainide, ajmaline, or pilsicainide, and the test was positive (coved-type ST elevation, Figure 2B) in 5 (shown with + in Figure 1). Thus, the diagnosis of BrS was established in 9/41 mutation carriers (1 individual showed spontaneous saddle-back ST elevation which was converted to coved-type by ajmaline).

SND was common in the cohort, presenting in 16/41 mutation carriers (Figure 2C), and 4 of these 16 carriers with SND also exhibited the BrS phenotype (Figures 2B, D). Moreover, 1 carrier showed SND without manifesting QT prolongation or ST elevation. Four patients received a permanent pacemaker and 3 received an implantable cardioverter defibrillator.

Biophysical Properties and Membrane Trafficking of E1784K

Whole-cell patch clamp recording showed that E1784K has the following biophysical abnormalities: (1) significantly smaller peak current density, (2) persistent Na current, (3)

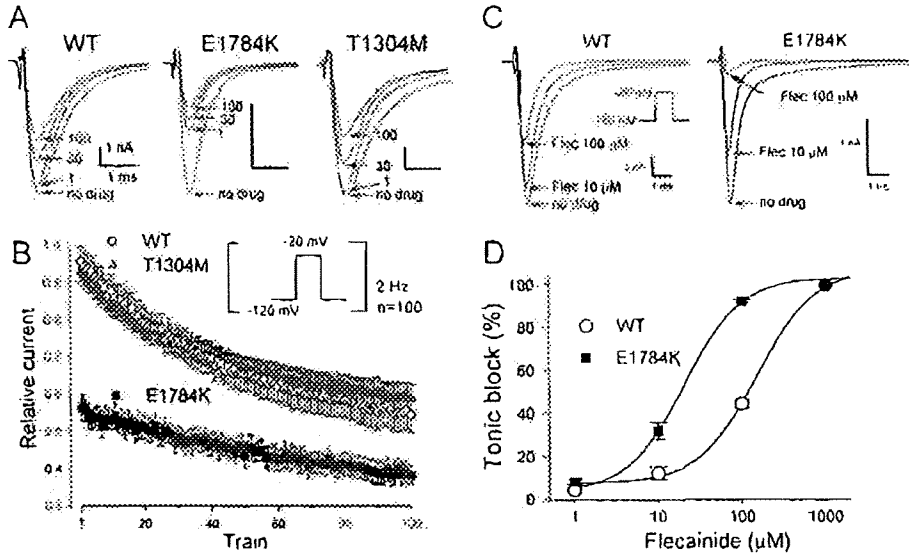

Figure 4. Tonic block, use-dependent block, and the dose-dependence of flecainide (A) Representative current traces of wild-type (WT), E1784K, and T1304M before and after 10 μmol/L flecainide. A train of 100 pulses (to −20 mV for 20 ms) was applied at 2 Hz from a holding potential of −120 mV. Numbers indicate the 1st (1), 30th (30), and 100th (100) pulse of the train. (B) Time course of the peak current levels after application of 10 μmol/L flecainide. Peak current levels recorded with each pulse were normalized to the baseline prior to flecainide. (C) Representative steady-state current traces of WT and E1784K before and after flecainide (10 and 100 μmol/L). Cells were depolarized by −20 mV from a holding potential of −150 mV. (D) Concentration-response curve for flecainide-induced tonic block in wild-type (WT) and E1784K. The normalized peak currents were fitted to the Hill equation. The IC_{50} values, representing dissociation constants for resting state were: WT, 150.3 μmol/L, E1784K, 20.4 μmol/L. Thus, the mutant channel was far more sensitive to tonic block by flecainide. (Modified with permission from Makita et al. *J Clin Invest* 2008; 118: 2219–2229[41])

Table 3. Reported Biophysical Properties of LQT3 Mutations

	SCN5A mutations				
	1795insD	ΔKPQ	ΔR1508	E1784K	T1304M
Clinical features					
QT prolongation	+	+	+	+	+
ST elevation*	+	+	+	+	−
Sinus node dysfunction	+	+	+	+	−
Biophysical and pharmacological properties					
Persistent Na current	+	+	+	+	+
Shift of $V_{1/2}$ (inactivation)	Negative	Negative	Negative	Negative	Positive
Shift of $V_{1/2}$ (activation)	Positive	Positive	Positive	Positive	Positive
Current decay	Slower	Faster	↔	Faster	Faster
Recovery from inactivation	Slower	Faster	ND	↔	Faster
Slow inactivation	Enhanced	↔	ND	Enhanced	↔
Tonic block by flecainide	Enhanced	Enhanced	Enhanced	Enhanced	↔
UDB by flecainide	Enhanced	Enhanced	ND	Diminished	↔
References	32, 33, 38, 66	3, 41, 67	37	40, 41	13, 41

*Spontaneous or Na-channel blocker-induced ST elevation; ↔ comparable to wild type.
ND, not determined.
Modified with permission from Makita et al. *J Clin Invest* 2008; 118: 2219–2229[41]

significantly faster macroscopic current decay, (4) hyperpolarizing shift of the steady-state inactivation, (5) significant depolarizing shift in the voltage-dependence of activation, and (6) normal recovery from inactivation (Figure 3). Furthermore, using a Na channel plasmid construct with an extracellular FLAG epitope, membrane trafficking of E1784K determined by a confocal laser scanning microscopy was comparable to the wild-type (WT). These observations provide strong evidence that the loss-of-function properties displayed by E1784K are most likely attributable to the aforementioned changes in gating properties rather than a change in channel density.

Molecular Mechanisms of Enhanced Flecainide Sensitivity

Class IC drug challenge test was positive in 56% patients with E1784K. Tonic block and use-dependent block by flecainide in WT and E1784K channels have been investigated, and compared with those of T1304M, a mutation that did not

show ST elevation during flecainide challenge test[35] Cells transfected with WT, E1784K, or T1304M were depolarized by 2 Hz pulse trains in the absence or presence of 10 μmol/L flecainide. During exposure to flecainide, peak currents normalized to predrug baseline were progressively reduced by the repetitive pulses (Figures 4A,B). There was a remarkable difference in the extent of first pulse (tonic) block that was only 4.5±4.0% for WT, and 7.1±2.7% for T1304M, compared with substantial tonic block in E1784K (43.7± 8.0%, P<0.001). Conversely, use-dependent block, determined by the difference in peak current values between the 1st and 100th test pulses relative to the 1st pulse, was slightly attenuated in E1784K. The net effect of flecainide after a train of 100 pulses was significantly greater in E1784K than in WT, but not in T1304M. Moreover, dose-response curves for flecainide block measured at a holding potential of −150 mV (thus representing drug affinity for the resting state) showed that the E1784K channels were 7.5-fold more sensitive to resting-state block by flecainide than were the WT channels (IC_{50}: WT=150.3 μmol/L, E1784K=20.4 μmol/L) (Figures 4C,D). These results indicate that the E1784K channels are much more sensitive to blocking by flecainide than are the WT and T1304M channels, and that this augmented sensitivity is attributable to enhanced tonic block rather than a change in use-dependent block.

Functional Determinants of LQT3 Associated With BrS and SND

To explore the functional determinants for the phenotypic overlap of BrS in LQT3 patients, the biophysical and pharmacological properties of reported LQT3 mutations were compared, and features commonly and specifically observed in those manifesting a BrS phenotype were sought (Table 3). The overlapping phenotype (LQT3 and BrS) has been previously reported for 1795insD[32,33] ΔKPQ[35,36] ΔK1500[37] and E1784K[35] In contrast, a carrier of T1304M did not show ST elevation during a flecainide test[35] Similarly, SND has been reported in carriers of the same *SCN5A* mutations, 1795insD[38] ΔKPQ[39] ΔK1500[37] E1784K[40] and D1790G[24] but not in other *SCN5A* mutations, including T1304M. Thus, it is plausible to speculate that the biophysical characteristics common to these mutations, but not found in T1304M, are channel properties responsible for evoking the mixed phenotypes of BrS and SND in patients with LQT3. Table 3 is a comparison of the functional properties of E1784K, and those reported for 1795insD, ΔKPQ, ΔK1500, E1784K, and T1304M[13] Among the biophysical properties listed in Table 3, both the negative-shift in steady-state inactivation, and the enhanced tonic block by flecainide are common to 1795insD, ΔKPQ, ΔK1500, and E1784K, but not to T1304M. This negative shift of inactivation will reduce the availability of the channels at the resting membrane potential, and increase the proportion of inactivated channels in both the open and closed state, reducing the Na current and increasing the sensitivity to Na-channel blockers. A positive shift in activation is another "loss-of-function" property evident in all the mutants, including T1304M, making it less likely that this specific channel property underlies the mixed clinical phenotypes in LQT3. Other channel properties, such as current decay, recovery from inactivation, slow inactivation or use-dependent block, were not common among 1795insD, ΔKPQ, ΔK1500, and E1784K.

A negative shift in inactivation is observed in E1784K, 1795insD, ΔKPQ, and ΔK1500, and may play a role in the overlap of the LQT3 clinical phenotype with BrS and SND in the mutation carriers, although the number of LQT3 mutations that have been evaluated in this detail is still small, the biophysical and pharmacological properties presented in a cultured cell line may not necessarily reflect the situation in vivo, and the effects of the mutation may be different in ventricular myocytes vs sinus node cells. Further studies that combine clinical and in vitro phenotyping in LQT3 mutations with and without overlapping clinical phenotypes will be required to confirm these findings. Nevertheless, a negative shift in inactivation and enhanced tonic block are common biophysical properties observed among *SCN5A* mutations in the LQT3/BrS overlapping phenotype.

Conclusions

E1784K is the most common LQT3 mutation. In patients with this and other LQT3 mutations, overlap of BrS and SND is relatively common. In vitro studies with E1784K and previous reports of LQT3 mutations with and without this clinical overlap syndrome implicate a negative shift in inactivation and enhanced tonic block by drugs as the underlying mechanisms. These findings suggest that patients with LQT3 mutations displaying these characteristics in vitro should not receive class IC drugs. Furthermore, they reinforce the general concept that in vitro characterization of the function of ion channel variants is a key component in generating specific therapeutic strategies for patient management.

Acknowledgments

The author thanks the following investigators, who were extensively involved in the international project "Functional characterization of the clinical overlap in cardiac sodium channelopathies"[21] for collecting clinical and genetic information of the LQT3 families, as well as the functional evaluation of the mutations: Elijah Behr (St George's University of London, UK), Wataru Shimizu (National Cardiovascular Center, Suita, Japan), Shigetomo Fukuhara and Naoki Mochizuki (National Cardiovascular Center Research Institute, Suita, Japan), Minoru Horie (Shiga University of Medical Science, Otsu, Japan), Akihiko Sunami (International University of Health and Welfare, Ohtawara, Japan), Lia Crotti and Peter J. Schwartz (University of Pavia, Pavia, Italy), Eric Schulze-Bahr (University of Muenster, Munster, Germany), and Alfred L. George Jr and Dan M. Roden (Vanderbilt University, Nashville, USA)

References

1. Catterall WA. From ionic currents to molecular mechanisms: The structure and function of voltage-gated sodium channels. *Neuron* 2000; 26: 13–25.
2. George AL Jr. Inherited disorders of voltage-gated sodium channels *J Clin Invest* 2005; 115: 1990–1999.
3. Bennett PB, Yazawa K, Makita N, George AL Jr. Molecular mechanism for an inherited cardiac arrhythmia *Nature* 1995; 376: 683–685
4. Shimizu W. Clinical impact of genetic studies in lethal inherited cardiac arrhythmias *Circ J* 2008; 72: 1926–1936.
5. Makita N, Horie M, Nakamura T, Ai T, Sasaki K, Yokoi H, et al. Drug-induced long-QT syndrome associated with a subclinical SCN5A mutation. *Circulation* 2002; 106: 1269–1274.
6. Chen Q, Kirsch GE, Zhang D, Brugada R, Brugada J, Brugada P, et al. Genetic basis and molecular mechanism for idiopathic ventricular fibrillation. *Nature* 1998; 392: 293–296.
7. Schott JJ, Alshinawi C, Kyndt F, Probst V, Hoorntje TM, Hulsbeek M, et al. Cardiac conduction defects associate with mutations in SCN5A. *Nat Genet* 1999; 23: 20–21
8. Benson DW, Wang DW, Dyment M, Knilans TK, Fish FA, Strieper MJ, et al. Congenital sick sinus syndrome caused by recessive mutations in the cardiac sodium channel gene (SCN5A) *J Clin Invest* 2003; 112: 1019–1028.
9. Groenewegen WA, Firouzi M, Bezzina CR, Vliex S, van Langen IM, Sandkuijl L, et al. A cardiac sodium channel mutation cosegregates

with a rare connexin40 genotype in familial atrial standstill. *Circ Res* 2003; 92: 14–22
10. Makita N, Sasaki K, Groenewegen WA, Yokota T, Yokoshiki H, Murakami T, et al. Congenital atrial standstill associated with coinheritance of a novel SCN5A mutation and connexin 40 polymorphisms. *Heart Rhythm* 2005; 2: 1128–1134.
11. Takehura N, Makita N, Kawabe J, Sato N, Kawamura Y, Kitabatake A, et al. A cardiac sodium channel mutation identified in Brugada syndrome associated with atrial standstill. *J Intern Med* 2004; 255: 137–142.
12. Wang DW, Viswanathan PC, Balser JR, George AL Jr, Benson DW. Clinical, genetic, and biophysical characterization of SCN5A mutations associated with atrioventricular conduction block. *Circulation* 2002; 105: 341–346.
13. Wang DW, Desai RR, Crotti L, Arnestad M, Insolia R, Pedrazzini M, et al. Cardiac sodium channel dysfunction in sudden infant death syndrome. *Circulation* 2007; 115: 368–376.
14. Otagiri T, Kijima K, Osawa M, Ishii K, Makita N, Matoba R, et al. Cardiac ion channel gene mutations in sudden infant death syndrome. *Pediatr Res* 2008; 64: 482–487.
15. Ackerman MJ, Siu BL, Sturner WQ, Tester DJ, Valdivia CR, Makielski JC, et al. Postmortem molecular analysis of SCN5A defects in sudden infant death syndrome. *JAMA* 2001; 286: 2264–2269.
16. Olson TM, Michels VV, Ballew JD, Reyna SP, Karst ML, Herron KJ, et al. Sodium channel mutations and susceptibility to heart failure and atrial fibrillation. *JAMA* 2005; 293: 447–454.
17. Darbar D, Kannankeril PJ, Donahue BS, Kucera G, Stubblefield T, Haines JL, et al. Cardiac sodium channel (SCN5A) variants associated with atrial fibrillation. *Circulation* 2008; 117: 1927–1935.
18. Ge J, Sun A, Paajanen V, Wang S, Su C, Yang Z, et al. Molecular and clinical characterization of a novel SCN5A mutation associated with atrioventricular block and dilated cardiomyopathy. *Circ Arrhythmia Electrophysiol* 2008; 1: 83–92.
19. McNair WP, Ku L, Taylor MRG, Fain PR, Dao D, Wolfel E, et al. SCN5A mutation associated with dilated cardiomyopathy, conduction disorder, and arrhythmia. *Circulation* 2004; 110: 2163–2167.
20. Watanabe H, Koopmann TT, Le Scouarnec S, Yang T, Ingram CR, Schott JJ, et al. Sodium channel beta1 subunit mutations associated with Brugada syndrome and cardiac conduction disease in humans. *J Clin Invest* 2008; 118: 2260–2268.
21. Keating MT. The long QT syndrome: A review of recent molecular genetic and physiologic discoveries. *Medicine (Baltimore)* 1996; 75: 1–5.
22. Wang Q, Shen J, Splawski I, Atkinson D, Li Z, Robinson JL, et al. SCN5A mutations associated with an inherited cardiac arrhythmia, long QT syndrome. *Cell* 1995; 80: 805–811.
23. Schwartz PJ, Priori SG, Locati EH, Napolitano C, Cantu F, Towbin JA, et al. Long QT syndrome patients with mutations of the SCN5A and HERG genes have differential responses to Na+ channel blockade and to increases in heart rate. Implications for gene-specific therapy. *Circulation* 1995; 92: 3381–3386.
24. Benhorin J, Taub R, Goldmit M, Kerem B, Kass RS, Windman I, et al. Effects of flecainide in patients with new SCN5A mutations: Mutation-specific therapy for long-QT syndrome? *Circulation* 2000; 101: 1698–1706.
25. Schwartz PJ. The congenital long QT syndromes from genotype to phenotype: Clinical implications. *J Intern Med* 2006; 259: 39–47.
26. Brugada P, Brugada J. Right bundle branch block, persistent ST segment elevation and sudden cardiac death: A distinct clinical and electrocardiographic syndrome: A multicenter report. *J Am Coll Cardiol* 1992; 20: 1391–1396.
27. Wilde AA, Antzelevitch C, Borggrefe M, Brugada J, Brugada R, Brugada P, et al. Proposed diagnostic criteria for the Brugada syndrome. *Eur Heart J* 2002; 23: 1648–1654.
28. Antzelevitch C. The Brugada syndrome: Ionic basis and arrhythmia mechanisms. *J Cardiovasc Electrophysiol* 2001; 12: 268–272.
29. Tan HL, Bink-Boelkens MT, Bezzina CR, Viswanathan PC, Beaufort-Krol GC, van Tintelen PJ, et al. A sodium-channel mutation causes isolated cardiac conduction disease. *Nature* 2001; 409: 1043–1047.
30. Shirai N, Makita N, Sasaki K, Yokoi H, Sakuma I, Sakurada H, et al. A mutant cardiac sodium channel with multiple biophysical defects associated with overlapping clinical features of Brugada syndrome and cardiac conduction disease. *Cardiovasc Res* 2002; 53: 348–354.
31. Makiyama T, Akao M, Tsuji K, Doi T, Ohno S, Takenaka K, et al. High risk for bradyarrhythmic complications in patients with Brugada syndrome caused by *SCN5A* gene mutations. *J Am Coll Cardiol* 2005; 46: 2100–2106.
32. Veldkamp MW, Viswanathan PC, Bezzina C, Baartscheer A, Wilde AA, Balser JR. Two distinct congenital arrhythmias evoked by a multidysfunctional Na+ channel. *Circ Res* 2000; 86: E91–E97.
33. Bezzina C, Veldkamp MW, van Den Berg MP, Postma AV, Rook MB, Viersma JW, et al. A single Na+ channel mutation causing both long-QT and Brugada syndromes. *Circ Res* 1999; 85: 1206–1213.
34. Viswanathan PC, Bezzina CR, George AL Jr, Roden DM, Wilde AA, Balser JR. Gating-dependent mechanisms for flecainide action in SCN5A-linked arrhythmia syndromes. *Circulation* 2001; 104: 1200–1205.
35. Priori SG, Napolitano C, Schwartz PJ, Bloise R, Crotti L, Ronchetti E. The elusive link between LQT3 and Brugada syndrome: The role of flecainide challenge. *Circulation* 2000; 102: 945–947.
36. Moss AJ, Windle JR, Hall WJ, Zareba W, Robinson JL, McNitt S, et al. Safety and efficacy of flecainide in subjects with long QT-3 syndrome (ΔKPQ mutation): A randomized, double-blind, placebo-controlled clinical trial. *Ann Noninvasive Electrocardiol* 2005; 10: 59–66.
37. Grant AO, Carboni MP, Neplioueva V, Starmer CF, Memmi M, Napolitano C, et al. Long QT syndrome, Brugada syndrome, and conduction system disease are linked to a single sodium channel mutation. *J Clin Invest* 2002; 110: 1201–1209.
38. Veldkamp MW, Wilders R, Baartscheer A, Zegers JG, Bezzina CR, Wilde AAM. Contribution of sodium channel mutations to bradycardia and sinus node dysfunction in LQT3 families. *Circ Res* 2003; 92: 976–983.
39. Moss AJ, Zareba W, Benhorin J, Locati EH, Hall WJ, Robinson JL, et al. ECG T-wave patterns in genetically distinct forms of the hereditary long QT syndrome. *Circulation* 1995; 92: 2929–2934.
40. Wei J, Wang DW, Alings M, Fish F, Wathen M, Roden DM, et al. Congenital long-QT syndrome caused by a novel mutation in a conserved acidic domain of the cardiac Na+ channel. *Circulation* 1999; 99: 3165–3171.
41. Makita N, Behr E, Shimizu W, Horie M, Sunami A, Crotti L, et al. The E1784K mutation in SCN5A is associated with mixed clinical phenotype of type 3 long QT syndrome. *J Clin Invest* 2008; 118: 2219–2229.
42. Splawski I, Shen J, Timothy KW, Lehmann MH, Priori S, Robinson JL, et al. Spectrum of mutations in long-QT syndrome genes: KVLQT1, HERG, SCN5A, KCNE1, and KCNE2. *Circulation* 2000; 102: 1178–1185.
43. Priori SG, Napolitano C, Gasparini M, Pappone C, Della Bella P, Brignole M, et al. Clinical and genetic heterogeneity of right bundle branch block and ST-segment elevation syndrome: A prospective evaluation of 52 families. *Circulation* 2000; 102: 2509–2515.
44. Shin DJ, Kim E, Park SB, Jang WC, Bae Y, Han J, et al. A novel mutation in the SCN5A gene is associated with Brugada syndrome. *Life Sci* 2007; 80: 716–724.
45. Juang JM, Huang SK, Tsai CT, Chiang FT, Lin JL, Lai LP, et al. Characteristics of Chinese patients with symptomatic Brugada syndrome in Taiwan. *Cardiology* 2003; 99: 182–189.
46. Zareba W, Sattar MN, Rosero S, Coudere JP, Moss AJ. Altered atrial, atrioventricular, and ventricular conduction in patients with the long QT syndrome caused by the DKPQ SCN5A sodium channel gene mutation. *Am J Cardiol* 2001; 88: 1311–1314.
47. Shin DJ, Jang Y, Park HY, Lee JE, Yang K, Kim E, et al. Genetic analysis of the cardiac sodium channel gene SCN5A in Koreans with Brugada syndrome. *J Hum Genet* 2004; 49: 573–578.
48. Chen T, Inoue M, Sheets MF. Reduced voltage dependence of inactivation in the SCN5A sodium channel mutation delF1617. *Am J Physiol Heart Circ Physiol* 2005; 288: H2666–H2676.
49. Smits JP, Koopmann TT, Wilders R, Veldkamp MW, Opthof T, Bhuiyan ZA, et al. A mutation in the human cardiac sodium channel (E161K) contributes to sick sinus syndrome, conduction disease and Brugada syndrome in two families. *J Mol Cell Cardiol* 2005; 38: 969–981.
50. Schulze-Bahr E, Eckardt L, Breithardt G, Seidl K, Wichter T, Wolpert C, et al. Sodium channel gene (SCN5A) mutations in 44 index patients with Brugada syndrome: Different incidences in familial and sporadic disease. *Hum Mutat* 2003; 21: 651–652.
51. Cordeiro JM, Barajas-Martinez H, Hong K, Burashnikov E, Pfeiffer R, Orsino AM, et al. Compound heterozygous mutations P336L and I1660V in the human cardiac sodium channel associated with the Brugada syndrome. *Circulation* 2006; 114: 2026–2033.
52. Rossenbacker T, Carroll SJ, Liu H, Kuipen C, de Ravel TJ, Devriendt K, et al. Novel pore mutation in SCN5A manifests as a spectrum of phenotypes ranging from atrial flutter, conduction disease, and Brugada syndrome to sudden cardiac death. *Heart Rhythm* 2004; 1: 610–615.
53. Itoh H, Shimizu M, Tanaka S, Mabuchi H, Imoto K. A novel missense mutation in the SCN5A gene associated with Brugada syndrome bidirectionally affecting blocking actions of antiarrhythmic drugs. *J Cardiovasc Electrophysiol* 2005; 16: 486–493.

54 Potet F, Mabo P, Le Coq G, Probst V, Schott JJ, Airaud F, et al. Novel brugada SCN5A mutation leading to ST segment elevation in the inferior or the right precordial leads. *J Cardiovasc Electrophysiol* 2003; **14**: 200–203.
55 Smits JP, Eckardt L, Probst V, Bezzina CR, Schott JJ, Remme CA, et al. Genotype-phenotype relationship in Brugada syndrome: Electrocardiographic features differentiate SCN5A-related patients from non-SCN5A-related patients. *J Am Coll Cardiol* 2002; **40**: 350–356.
56 Kyndt F, Probst V, Potet F, Demolombe S, Chevalier JC, Baro I, et al. Novel SCN5A mutation leading either to isolated cardiac conduction defect or Brugada syndrome in a large French family. *Circulation* 2001; **104**: 308–3086.
57 Tan BH, Valdivia CR, Song C, Makielski JC. Partial expression defect for the SCN5A missense mutation G1406R depends upon splice variant background Q1077 and rescue by mexiletine. *Am J Physiol Heart Circ Physiol* 2006; **291**: H1822–H1828.
58 Kehl HG, Haverkamp W, Rellensmann G, Yelbuz TM, Krasemann T, Vogt J, et al. Life-threatening neonatal arrhythmia. Successful treatment and confirmation of clinically suspected extreme long QT-syndrome-3 [Images in cardiovascular medicine]. *Circulation* 2004; **109**: e205–e205.
59 Chang CC, Acharfi S, Wu MH, Chiang FT, Wang JK, Sung TC, et al. A novel SCN5A mutation manifests as a malignant form of long QT syndrome with perinatal onset of tachycardia/bradycardia. *Cardiovasc Res* 2004; **64**: 268–278.
60 Tester DJ, Will ML, Haglund CM, Ackerman MJ. Compendium of cardiac channel mutations in 541 consecutive unrelated patients referred for long QT syndrome genetic testing. *Heart Rhythm* 2005; **2**: 507–517.
61 Valdivia CR, Ackerman MJ, Tester DJ, Wada T, McCormack J, Ye B, et al. A novel SCN5A arrhythmia mutation, M1766L, with expression defect rescued by mexiletine. *Cardiovasc Res* 2002; **55**: 279–289.
62 Ye B, Valdivia CR, Ackerman MJ, Makielski JC. A common human SCN5A polymorphism modifies expression of an arrhythmia causing mutation. *Physiol Genomics* 2003; **12**: 187–193.
63 Lupoglazoff JM, Cheav T, Baroudi G, Berthet M, Denjoy I, Cauchemez B, et al. Homozygous SCN5A mutation in long-QT syndrome with functional two-to- one atrioventricular block. *Circ Res* 2001; **89**: E16–E21.
64 Tester DJ, Ackerman MJ. Genetic testing for cardiac channelopathies: Ten questions regarding clinical considerations for heart rhythm allied professionals. *Heart Rhythm* 2005; **2**: 675–677.
65 Shim SH, Ito M, Maher T, Milunsky A. Gene sequencing in neonates and infants with the long QT syndrome. *Genet Test* 2005; **9**: 281–284.
66 Baroudi G, Chahine M. Biophysical phenotypes of SCN5A mutations causing long QT and Brugada syndromes. *FEBS Lett* 2000; **487**: 224–228.
67 Nagatomo T, January CT, Makielski JC. Preferential block of late sodium current in the LQT3 Delta KPQ mutant by the class IC antiarrhythmic flecainide. *Mol Pharmacol* 2000; **57**: 101–107.

THE JOURNAL OF BIOLOGICAL CHEMISTRY VOL. 284, NO. 50, pp. 35122–35133, December 11, 2009

Novel Mechanisms of Trafficking Defect Caused by *KCNQ1* Mutations Found in Long QT Syndrome*

Received for publication, May 5, 2009, and in revised form, October 7, 2009 Published, JBC Papers in Press, October 13, 2009, DOI 10.1074/jbc.M109.017293

Akinori Sato[‡§], Takuro Arimura[‡], Naomasa Makita[¶], Taisuke Ishikawa[‡], Yoshiyasu Aizawa[§], Hiroya Ushinohama[‖], Yoshifusa Aizawa[§], and Akinori Kimura[‡1]

From the [‡]Department of Molecular Pathogenesis, Medical Research Institute, Tokyo Medical and Dental University, 1-5-45 Yushima, Bunkyo-Ku, Tokyo 113-8510, Japan, the [§]Division of Cardiology, Niigata University Graduate School of Medical and Dental Sciences, Niigata 951-8510, Japan, the [¶]Department of Molecular Physiology-1, Nagasaki University Graduate School of Biomedical Sciences, Nagasaki 852-8523, Japan, and the [‖]Department of Pediatric Cardiology, Fukuoka Children's Hospital, Fukuoka 810-0063, Japan

Long QT syndrome (LQTS) is a hereditary arrhythmia caused by mutations in genes for cardiac ion channels, including a potassium channel, KvLQT1. Inheritance of LQTS is usually autosomal-dominant, but autosomal-recessive inheritance can be observed in patients with LQTS accompanied by hearing loss. In this study, we investigated the functional alterations caused by *KCNQ1* mutations, a deletion (delV595) and a frameshift (P631fs/19), which were identified in compound heterozygous state in two patients with autosomal-recessive LQTS not accompanied by hearing loss. Functional analyses showed that both mutations impaired cell surface expression due to trafficking defects. The mutations severely affected outward potassium currents without apparent dominant negative effects. It was found that delV595 impaired subunit binding, whereas P631fs/19 was retained in endoplasmic reticulum due to the newly added 19-amino acid sequence containing two retention motifs (R^{633}GR and R^{646}LR). This is the first report of novel mechanisms for trafficking abnormality of cardiac ion channels, providing us new insights into the molecular mechanisms of LQTS.

Long QT syndrome (LQTS)[2] is characterized by prolongation of QT interval in electrocardiogram (ECG), syncope, and sudden death due to polymorphic ventricular tachyarrhythmia (1). From the genetic viewpoints, LQTS is classified into two subtypes, Jervell and Lange-Nielsen syndrome (Online Mendelian Inheritance in Man (OMIM) 220400) and Romano Ward syndrome (OMIM 192500). The Jervell and Lange-Nielsen syndrome is defined as LQTS of the autosomal-recessive genetic trait, which is often accompanied by sensorineural deafness, whereas Romano Ward syndrome defines LQTS without deafness, which is inherited as the autosomal-dominant trait. Recent genetic analyses have revealed that most of the Jervell and Lange-Nielsen syndrome patients carried mutations in *KCNQ1* that encodes the α-subunit of a voltage-gated cardiac potassium channel, KvLQT1 (2). In contrast, Romano Ward syndrome can be caused by mutations in genes for potassium channels, including KvLQT1 and HERG, sodium channels, a calcium channel, and other molecules associated with cardiac ion channels (1, 3–6).

The α-subunit of KvLQT1 has the domain structure composed of six membrane-spanning segments (S1–S6) containing a pore region localized at cell membrane and the N-terminal and C-terminal regions that are localized in the cytoplasm. The KvLQT1 channel consists of four α-subunits (7) and two β-subunits (MinK) encoded by *KCNE1* (8), which generates slow component of delayed rectifier potassium current (I_{Ks}). Many *KCNQ1* mutations associated with Jervell and Lange-Nielsen syndrome and Romano Ward syndrome have been reported, most of which were found in the membrane-spanning segments and impaired the channel function (1). There are several other mutations not affecting the pore structure but causing functional impairment, most of which were identified in the C-terminal cytoplasmic region. Although the cytoplasmic region contained several functional domains (9–12), molecular mechanisms of *KCNQ1* mutations in the cytoplasmic domain have not been fully elucidated.

On the other hand, more information is available about the functional alterations caused by mutations in *KCNH2* that encodes pore-forming α-subunits of another voltage-gated cardiac potassium channel, HERG. The α-subunits form the tetrameric channel complex in the endoplasmic reticulum (ER) (13–15), and the tetramer is glycosylated in ER and Golgi body (16) and then transported to and expressed at the cell membrane. The HERG channel generates rapid component of the delayed rectifier potassium current (I_{Kr}) (5). With regard to the functional alterations caused by *KCNH2* mutations associated with Romano Ward syndrome, most mutations in the cytoplasmic regions caused trafficking defects due to misfolding in ER (17) or the failure of transport from ER to Golgi body (18). These functional abnormalities decreased the I_{Kr} current in the cardiomyocytes and led to the prolongation of repolarizing

* This work was supported in part by grants-in-aid from the Ministry of Education, Culture, Sports, Science, and Technology, Japan, grants from the Japan-Korea Collaboration Program and from the Japan-France Collaboration Program from the Japan Society for Promotion of Science, and research grants from the Ministry of Health, Labor, and Welfare, Japan.

[1] To whom correspondence should be addressed: 1-5-45 Yushima, Bunkyo-Ku, Tokyo 113-8510, Japan. Tel.: 81-3-5803-4905; Fax: 81-3-5803-4907; E-mail: akitis@mri.tmd.ac.jp.

[2] The abbreviations used are: LQTS, long QT syndrome; ECG, electrocardiogram; I_{Ks}, slow component of delayed rectifier potassium current; ER, endoplasmic reticulum; I_{Kr}, rapid component of the delayed rectifier potassium current; QTc, corrected QT; WT, wild-type; aa, amino acid(s); EGFP, enhanced green fluorescent protein; co-IP, co-immunoprecipitation; Ab, antibody; PBS, phosphate-buffered saline; HRP, horseradish peroxidase; AU, arbitrary units; pF, picofarad; K_{ATP}, ATP-sensitive potassium.

TABLE 1
Primers used for cloning

Production	Forward primer (5′–3′)	Reverse primer (5′–3′)
KvLQT1-WT	GCTCGGATCCGTTATGGCCGC	GGATATCTGCAGAATTCGGC
L1-Myc-KvLQT1	GCTGTCCACCATCGAGGAGCAGAAACTCATCTCTGA AGAGGATCTGCAGTATGCCGCCCTGGC	GCCAGGGCGGCATACTGCAGATCCTCTTCAGAGATGAG TTTCTGCTCCTCGATGGTGGACAGC
C terminus KvLQT1	GGGGATCCATCGGGCCACCATTAAGGTCATT	CTTGCGGCCGCCAGCCCCATCCCCTCCTCA
KvLQT1-delV595	CGCCTGAACCGAGAAGAC	CGTCACCTTGTCTTCTCGG
KvLQT1-P631fs/19	GCGGCCCCCCCCAGAGAG	CCCTCTCTGGGGGGGGCC
KvLQT1-AAA/RLR	CCCCAGGCAGCTGCGGGCCCACATCAC	GTGGGCCCGCAGCTGCCTGGGGGGGGCC
KvLQT1-RGR/AAA	CCTGCGGCAGTGGGCTGCAGCTCGACC	GCTCAGGGTCGAGCTGCAGCCCACTGC
KvLQT1-P631stop	GCTCGGATCCGTTATGGCCGC	CCGAATTCTCAGGGGGGGCC
KvLQT1-P631fs2/34	GCGGCCCCCCCCCAGAGAG	CCCTCTCTGGGGGGGGGCC
KvLQT1-R594Q	CGCCCGCCTGAACCAAGTAGAAG	ACCTTGTCTTCTACTTGGTTCAG

phase of action potential, manifested with prolonged QT interval in the ECG (19).

In this study, we investigated functional alterations caused by two mutations, delV595 and P631fs/19, in the C-terminal region of the KvLQT1 channel, which were found in an LQTS family of autosomal-recessive inheritance. It was demonstrated that both mutations lead to trafficking defects, resulting in the loss of channel function. This is the first report on two novel mechanisms of channel-trafficking abnormalities: an impaired subunit binding and a newly generated ER retention signal.

EXPERIMENTAL PROCEDURES

Case Presentation—The proband of the LQTS family was a 10-year-old girl with a history of cardiopulmonary arrest during exercise. Ventricular fibrillation was confirmed when she was revived by cardiopulmonary resuscitation. Her ECG showed a wide T-wave and prolonged corrected QT (QTc) interval (0.55 s). Her eldest brother also suffered from LQTS. He experienced syncope during exercise at the age of 13. His ECG after the event showed T-wave alternans, and prolongation of QTc interval (0.48 s) was found even at rest. Neither patient had any history of hearing loss. Prolongation of QTc interval was not found in the ECGs of either the parents or the second eldest brother. The other relatives of this family had no history of syncope or sudden death.

Genetic Analysis—The research protocol was approved by the Ethics Reviewing Committee of the Medical Research Institute, Tokyo Medical and Dental University. Genetic screening was performed for the proband and her family members. The control subjects were 180 genetically unrelated Japanese individuals who were selected at random. Blood samples were obtained from each subject, who provided informed consent for the clinical and genetic studies. Genomic DNA was extracted from peripheral blood samples by conventional methods. Each exon of *KCNQ1*, *KCNH2*, *SCN5A*, *KCNE1*, *KCNE2*, and *KCNJ2* genes was amplified by PCR. The PCR products were analyzed by direct sequencing using Big Dye Terminator chemistry (Applied Biosystems) according to the manufacturer's instructions. Sequences of primers used in the genetic analyses are available on request.

Alignment of Amino Acid Sequences and Prediction of Tertiary Structure—Amino acid sequences of human KvLQT1 protein predicted from nucleotide sequences (GenBank™ NM_000218) were aligned with those of bovine (XM_001252337), dog (XM_540790), rat (NM_032073), mouse (NM_008434), and chicken (XM_421022), using GENETIX version 8.1.2 software (Genetics, Tokyo, Japan). The tertiary structure of coiled-coil was predicted by using COILS (available on the World Wide Web) (20).

Electrophysiological Studies—Wild-type (WT) full-length *KCNQ1* (NM_000218) and *KCNE1* (NM_000219) cDNA fragments corresponding to aa 1–676 and aa 1–129, respectively, were amplified by reverse transcription-PCR from human heart cDNA. Mutant *KCNQ1* cDNA fragments carrying deletion of GTA (delV595 mutation) or insertion of C (P631fs/19 mutation) were generated by the primer-directed mutagenesis method. The *KCNQ1* cDNA fragments were cloned in the bicistronic plasmid pIRES2-EGFP (Clontech, Mountain View, CA) to make pIRES2-EGFP-KvLQT1 constructs, whereas *KCNE1* cDNA was inserted into the bicistronic plasmid pCD8-IRES to make the pCD8-IRES-MinK construct. All of the constructs used in this study were sequenced to ensure that no error was introduced. Sequences of the primers used in the plasmid construction are listed in Table 1.

CHO-K1 cells were transiently transfected using Lipofectamine (Invitrogen) with a pIRES2-EGFP-KvLQT1 plasmid (0.75 μg) of either WT or mutant in combination with the pCD8-IRES-MinK plasmid (0.75 μg) to visually identify the cells expressing heterologous KvLQT1 with EGFP under a fluorescent microscope and MinK with Dynabeads M-450 CD8 (Invitrogen), respectively. Potassium currents were recorded from cells that were positive for both EGFP and CD8 using the whole-cell patch clamp techniques as described previously (21). Currents were recorded using an Axopatch 200A amplifier (Axon Instruments, Foster City, CA), and series resistance errors were reduced by 60–70% using electronic compensation. Holding potential was −80 mV. All of the signals were acquired at 5–500 kHz (Digidata 1322, Axon Instruments) with a personal computer running Clampex 9 software (Axon Instruments) and filtered at 5 kHz with a 4-pole Bessel low pass filter. Membrane currents were analyzed with Clampfit 9 software (Axon Instruments).

Co-immunoprecipitation (co-IP) Assay—The cDNA fragments corresponding to the C terminus of KvLQT1 (aa 353–676) were generated for WT, delV595, and P631fs/19 by PCR from the *KCNQ1* plasmids described earlier. Another mutant cDNA containing a substitution of G with A (R594Q mutation) was obtained from the KvLQT1-WT construct by the primer-directed mutagenesis method. The cDNA fragments corresponding to the C terminus of KvLQT1 were cloned into

pCMV-Tag3C (Stratagene, Cedar Creek, TX) and pBIND (Promega, Madison, WI).

The co-IP assays were performed as previously described (22, 23). Briefly, COS-7 cells or HEK293 cells were co-transfected with a combination of pCMV-Tag3C-KvLQT1 (Myc-tagged C terminus KvLQT1) and pBIND-KvLQT1 (GAL4-tagged C terminus KvLQT1) constructs to analyze the binding of KvLQT1 subunits. Aliquots of the cellular extracts were collected for assessing the expression levels, and the remaining supernatants containing equal amount of proteins were used for the co-IP assay using the Catch and Release version 2.0 reversible immunoprecipitation system, according to the manufacturer's instructions (Millipore, Billerica, MA), with mouse anti-GAL4 monoclonal antibody (Ab) (Santa Cruz Biotechnology, Inc., Santa Cruz, CA). Eluted samples were separated by SDS-PAGE, transferred to a nitrocellulose membrane, preincubated with 5% skimmed milk in phosphate-buffered saline (PBS), and incubated with primary rabbit anti-c-Myc polyclonal Ab (1:100; Santa Cruz Biotechnology, Inc.) or rabbit anti-GAL4 polyclonal Ab (1:100; Santa Cruz Biotechnology, Inc.) followed by secondary goat anti-rabbit (for polyclonal Ab) IgG HRP-conjugated Ab (1:1000; Dako A/S, Grostrup, Denmark). The signals were visualized by Immobilon Western Chemiluminescent HRP substrate (Millipore) and luminescent image analyzer LAS-3000mini (Fujifilm, Tokyo, Japan). The densitometric intensities were measured as means by using Multi Gauge version 3.0 (Fujifilm).

Protein Expression and Subcellular Fraction Assays—KvLQT1-WT, -delV595, and -P631fs/19 cDNA fragments were cloned into pCMV-Tag3B (Stratagene) to add a Myc tag at the N terminus of KvLQT1 (Nt-Myc-KvLQT1) or into pEGFP-C1 (Clontech) to add a green fluorescent protein (GFP) tag (GFP-KvLQT1). HEK293 cells (1.0×10^6) were seeded onto a poly-D-lysine-coated 60-mm dish (BD Biosciences). After 24 h, 1 μg of Nt-Myc-KvLQT1 and 1 μg of Myc-tagged C terminus KvLQT1 constructs were added to the dish with TransFectin lipid reagent (Bio-Rad). After 12, 24, 48, and 72 h of transfection, the cells were subjected to sonication in 2% SDS, 250 mM sucrose, 75 mM urea, 1 mM dithiothreitol, and 50 mM Tris-HCl, pH 7.5, and the protease inhibitor mixture (Sigma). After measuring the protein concentration by using BCA protein assay regent (Pierce), equal amounts of proteins were subjected to SDS-PAGE and experiments using Western blotting. The membrane was incubated with primary mouse anti-glyceraldehyde-3-phosphate dehydrogenase monoclonal Ab (1:100; Santa Cruz Biotechnology, Inc.) or rabbit anti-c-Myc polyclonal Ab (1:100; Santa Cruz Biotechnology, Inc.), followed by incubation with appropriate secondary Ab: rabbit anti-mouse IgG HRP-conjugated Ab (1:1000; Dako A/S) or goat anti-rabbit IgG HRP-conjugated Ab (1:1000; Dako A/S).

For the subcellular fraction assay, Nt-Myc-KvLQT1 or GFP-KvLQT1 constructs were transfected into HEK293 cells plated on a poly-D-lysine-coated 60-mm dish (BD Biosciences). After 48 h, cells were subjected to brief sonication in 150 mM NaCl, 1 mM EDTA, and 10 mM Tris-HCl, pH 7.6, containing 1% Triton X-100 and the protease inhibitor mixture. The cell lysates were centrifuged at 15,000 rpm for 15 min at 4 °C to remove cell debris, nuclei, and large particulates. The supernatant portion containing both the membrane proteins and cytosolic proteins was collected and further centrifuged at 40,000 rpm for 30 min at 4 °C to separate the membrane fraction from the cytosolic fraction as described by Wu *et al.* (24). The supernatant (cytosolic fraction) was removed after the centrifugation, and the pellet (membrane fraction) was subjected to the sonication in 2% SDS, 250 mM sucrose, 75 mM urea, 1 mM dithiothreitol, and 50 mM Tris-HCl, pH 7.5, and the protease inhibitor mixture. After measuring the protein concentration by using BCA reagent, equal amounts of proteins were subjected to the SDS-PAGE and Western blot analysis. The membrane was incubated with primary rabbit anti-c-Myc polyclonal Ab (1:100; Santa Cruz Biotechnology), mouse anti-GFP monoclonal Ab (1:1000; Clontech), or mouse anti-caveolin-1 monoclonal Ab (1:1000; BD Biosciences), followed by the incubation with the appropriate secondary Ab. Signals were visualized, and the densitometric intensities were measured as described earlier.

Immunofluorescence Microscopy—Mutant cDNA fragments containing substitution of AGA with TGA (P631stop mutation) or insertion of CC (P631fs2/34 mutation) were obtained by the primer-directed mutagenesis method from the KvLQT1-WT construct. We also constructed the P631fs/19-mutant carrying $A^{633}AA + R^{646}LR$, $R^{633}GR + A^{646}AA$, or $A^{633}AA + A^{646}AA$ by primer-directed mutagenesis from the KvLQT1-P631fs/19 construct. All of the constructs were cloned into the pcDNA3.1(+) vector (Invitrogen). To introduce a c-Myc epitope (EQKLISEEDL) into the extracellular linker 1 (L1) between the S1 and S2 after the position of aa 146 of each KvLQT1 construct, we used a recombination PCR, and the PCR fragment was introduced into the pcDNA3.1(+)-based KvLQT1 constructs (L1-Myc-KvLQT1) (25).

HEK293 cells (7.0×10^4) were seeded onto poly-D-Lysine 8-well culture slides (BD Biosciences), and 24 h later, 0.3 μg of L1-Myc-KvLQT1 constructs or 0.15 μg of L1-Myc-KvLQT1 constructs plus 0.15 μg of MinK constructs were added into wells with 0.6 μl of TransFectin lipid reagent (Bio-Rad). After 48 h, the cells were washed with PBS, fixed in 4% paraformaldehyde and incubated with mouse anti-c-Myc monoclonal Ab (1:200; Santa Cruz Biotechnology, Inc.). After washing with PBS, Alexa Fluor 568 goat anti-mouse IgG_1 Ab (1:400; Invitrogen) in 3% bovine serum albumin was applied. To detect the intracellular L1-Myc-KvLQT1 protein, HEK293 cells fixed in 4% paraformaldehyde were permeabilized with 0.15% Triton X-100 in PBS with 3% bovine serum albumin. The permeabilized cells transfected with L1-Myc-KvLQT1 constructs were incubated with the primary and secondary Abs. The permeabilized cells transfected with L1-Myc-KvLQT1 constructs were also incubated with rabbit anti-calnexin polyclonal Ab (1:100; Sigma), Alexa Fluor 568 goat anti-mouse IgG_1 Ab, and sheep anti-rabbit IgG fluorescein isothiocyanate-conjugated Ab (1:400; Chemicon, Australia). To assess the efficacy of permeabilization, non-permeabilized and permeabilized cells were incubated with mouse anti-α-tubulin monoclonal Ab (1:1000; Sigma), and with Alexa Fluor 568 goat anti-mouse IgG_1 Ab that detected the intracellular protein α-tubulin only in the permeabilized cells. The transfected HEK293 cells were mounted on cover glass using Mowiol 4-88 reagent (Calbiochem) with or without 4′,6-diamidino-2-phenylindole. Images were collected

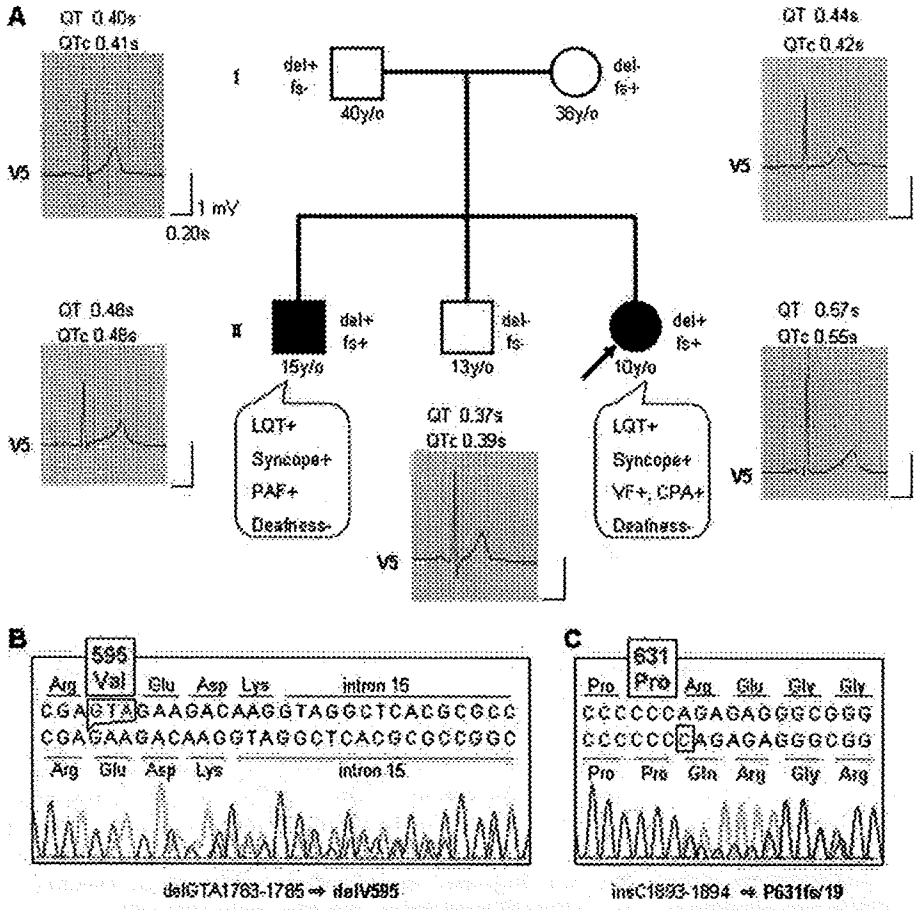

FIGURE 1. **Pedigree of an LQTS family carrying *KCNQ1* mutations.** *A*, clinical finding, ECG finding, and *KCNQ1* genotype of each member in the LQTS family. The *filled square* and *filled circle* indicate affected male and female, respectively. The *open squares* and *open circle* represent unaffected males and female, respectively. The *arrow* indicates the proband. The presence or absence of *KCNQ1* mutations, delGTA1783–1785 (delV595) and insC1893–1894 (P631fs/19), is indicated as *del+* or *del−* and *fs+* or *fs−*, respectively. ECGs of V5 lead at rest and its QT and corrected QT (QTc) intervals are shown. The clinical characteristics of each member are also indicated. *y/o*, years old; *LQT*, QT prolongation; *PAF*, paroxysmal atrial fibrillation; *VF*, ventricular fibrillation; *CPA*, cardiopulmonary arrest. *B* and *C*, direct sequencing data from the proband. Deletion of GTA should result in deletion of valine at codon 595 (*B*), and insertion of C was predicted to cause a frameshift after proline at codon 631 (*C*).

and analyzed with a laser confocal microscope (LSM510, Carl Zeiss (Jena, Germany)).

Luminometric Surface Expression Assay—In the luminometric surface expression assay, we tested L1-Myc-KvLQT1-WT, -delV595, -P631fs/19, -P631stop, -P631fs2/34, and -P631fs/19 derivatives; Nt-Myc-KvLQT1-WT; and Myc(−)-KvLQT1-WT. The assay was performed as previously described (26). Briefly, HEK293 cells were seeded at 2.0×10^5 in each well of a poly-D-lysine-coated multiwell plate (BD Biosciences). After 24 h, the cells were transfected with 0.6 μg of L1-Myc-KvLQT1 constructs, Nt-Myc-KvLQT1-WT, or Myc(−)-KvLQT1-WT along with 0.6 μg of MinK cDNA and 1.2 μl of TransFectin lipid reagent (Bio-Rad). After 48 h of transfection, the living cells were incubated with primary mouse anti-c-Myc monoclonal Ab (1:200; Santa Cruz Biotechnology) at 37 °C for 2 h, followed by fixation in 4% paraformaldehyde. After washing three times with PBS, the cells were incubated with the secondary rabbit anti-mouse IgG HRP-conjugated Ab (1:2000; Dako) in 3% bovine serum albumin for 40 min at room temperature. After washing with PBS, the bottoms of the wells were dipped with Immobilon Western Chemiluminescent HRP substrate (Millipore), and the plate was placed in the luminescent image analyzer LAS-3000mini (Fujifilm). The intensity of chemiluminescence from each well was measured with a densitometer using Multi Gauge version 3.0 (Fujifilm) and expressed as arbitrary units (AU).

Statistical Methods—Numerical data were expressed as means ± S.E. Statistical differences were analyzed using one-way analysis of variance and Student's *t* test for paired values. Means were compared by independent sample *t* tests without correction for multiple comparisons. A p value of <0.05 was considered statistically significant.

RESULTS

Identification of KCNQ1 Mutations in LQTS—Mutational analysis of cardiac ion channel genes in the proband of LQTS family (Fig. 1*A*) identified two different *KCNQ1* mutations, a deletion of three nucleotides at position 1783–1785 in exon 15, resulting in the predicted deletion of valine 595 (delV595) (Fig. 1*B*) and an insertion of cytosine between positions 1893 and 1894 in exon 16. This resulted in a frameshift mutation after the 631th residue (proline), which replaced the original 45 amino acids with 19 novel amino acids (P631fs/19) (Fig. 1*C*). Both mutations were not detected in 180 unrelated healthy Japanese individuals. The former mutation is newly described, whereas the latter mutation has been reported to be a cause of LQTS (27, 28). No mutation in the other LQT-causing genes, *KCNH2*, *SCN5A*, *KCNE1*, *KCNE2*, and *KCNJ2*, has been identified in the proband. A family study revealed that the affected eldest brother carried both mutations, whereas the unaffected second eldest brother carried no mutation. Each mutation was found in each parent: delV595 in the father and P631fs/19 in the mother (Fig. 1*A*). None of the family members suffered hearing loss.

Structure and Alignment of C Terminus of KvLQT1 around the Mutations—Valine 595 was located in four heptad repeats between aa 588 and 616, and evolutionarily conserved in the KvLQT1 channel among various species (Fig. 2*A*). Structures of WT, delV595, and P631fs/19 in this region were predicted by using the program COILS along with another LQTS-associated mutation R594Q (28). Two coiled-coil structures were predicted for WT, P631fs/19, and R594Q (Fig. 2, *B*, *D*, and *E*,

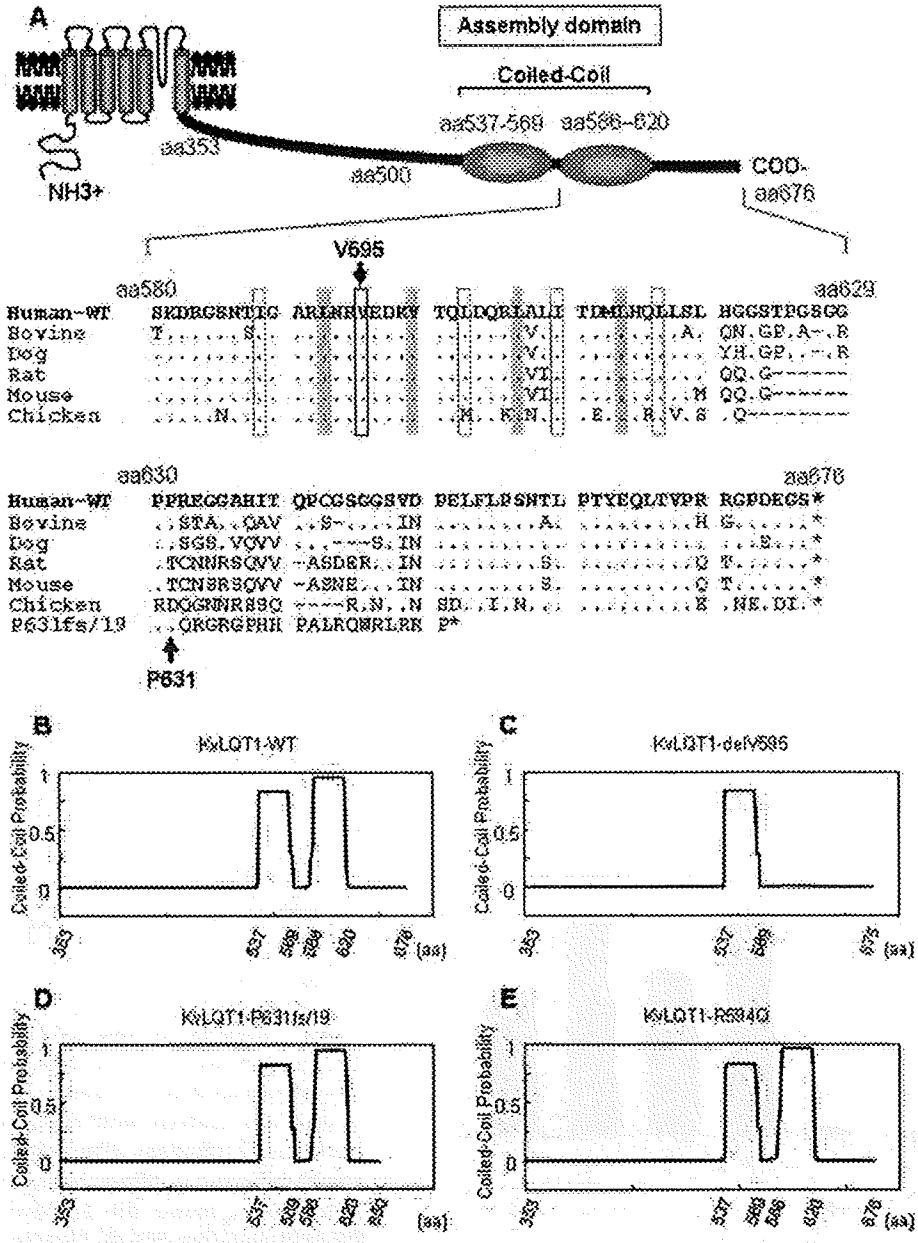

FIGURE 2. **Alignment of amino acid sequences around the mutations and predicted coiled-coil structure of KvLQT1 cytoplasmic region.** *A* (*top*), schematic representation of KvLQT1 α-subunit that has two coiled-coil structures (assembly domain) in the C-terminal region. *Bottom*, the alignment of amino acid sequences around the mutations. Amino acid sequences of human KvLQT1 (from aa 580 to 676) predicted from nucleotide sequences were aligned with those from bovine, dog, rat, mouse, and chicken. The *shadowed boxes* and *black open squares* indicate hydrophobic residues constituting heptad repeats. Additional amino acid sequences generated by the P631fs/19 mutation are also aligned. The *asterisks*, *dots*, and *dashes* indicate stop codons, identities to the human KvLQT1, and spaces introduced to obtain maximum homology, respectively. *B–E*, coiled-coil structure was predicted by using the COILS software for the KvLQT1 C-terminal cytoplasmic region, as shown for WT (*B*), delV595 (*C*), P631fs/19 (*D*), or R594Q (*E*). The probability at each position is shown as a *line* between 0 and 1.

respectively), whereas complete destruction of the second coiled-coil structure was predicted for delV595 (Fig. 2*C*).

Altered Electrophysiological Characters Caused by the Mutations—Whole-cell currents were recorded by a step pulse protocol from cells expressing EGFP and full-length KvLQT1-WT or -mutant in the presence of CD8-MinK (Fig. 3, *A* and *B*). KvLQT1-WT exhibited a slowly activating outward current similar to I_{Ks} (Fig. 3*C*). On the other hand, both KvLQT1-delV595 and KvLQT1-P631fs/19 produced little to no current (Fig. 3, *D* and *E*, respectively). Peak current densities measured at the test pulse of +60 mV were significantly smaller in cells expressing either delV595 (2.8 ± 0.6 pA/pF, $n = 4$; $p < 0.001$), P631fs/19 (2.6 ± 0.8 pA/pF, $n = 4$; $p < 0.001$), or delV595 + P631fs/19 (5.4 ± 2.2 pA/pF, $n = 3$; $p < 0.001$) than WT (130.0 ± 15.4 pA/pF, $n = 23$) (Fig. 3*F*). To investigate whether the mutant KvLQT1 channels would exhibit dominant negative suppression effects, KvLQT1-delV595 or KvLQT1-P631fs/19 was co-transfected with an equal amount of KvLQT1-WT in the presence of CD8-MinK. It was found that the co-expression of delV595 or P631fs/19 did not affect the peak current densities of KvLQT1-WT (WT + delV595: 145.8 ± 33.3 pA/pF, p = NS; WT + P631fs/19: 113.9 ± 16.4 pA/pF, p = NS), demonstrating that these mutations did not exert the dominant negative suppression (Fig. 3*F*). In addition, we examined the functional properties of KvLQT1-P631fs/19 carrying $A^{633}AA + A^{646}AA$ (AAA/AAA) that lacked both ER retention signals of $R^{633}GR$ and $R^{646}LR$ (details are described below). The AAA/AAA mutant exhibited peak current density comparable with that of KvLQT1-WT, either alone (AAA/AAA: 94.6 ± 16.2 pA/pF, $n = 5$, p = NS) or in combination with KvLQT1-WT (WT + AAA/AAA: 146.1 ± 27.2 pA/pF, $n = 11$, p = NS) (Fig. 3*F*).

Altered KvLQT1 Subunit Binding Caused by the Mutation delV595—To investigate the functional alterations caused by the *KCNQ1* mutations in the subunit assembly, we performed co-IP assays for KvLQT1-WT and -mutants. Myc-tagged C terminus KvLQT1-WT or -mutant (delV595, P631fs/19, or R594Q) constructs were co-transfected into COS-7 cells with GAL4-tagged C terminus KvLQT1-WT or -mutant construct (Fig. 4*A*). Western blot analyses of whole-cell supernatants demonstrated that these constructs expressed proteins at a similar level (Fig. 4*B*). To evaluate the binding of each subunit, we measured the amount of Myc-tagged proteins immunopre-

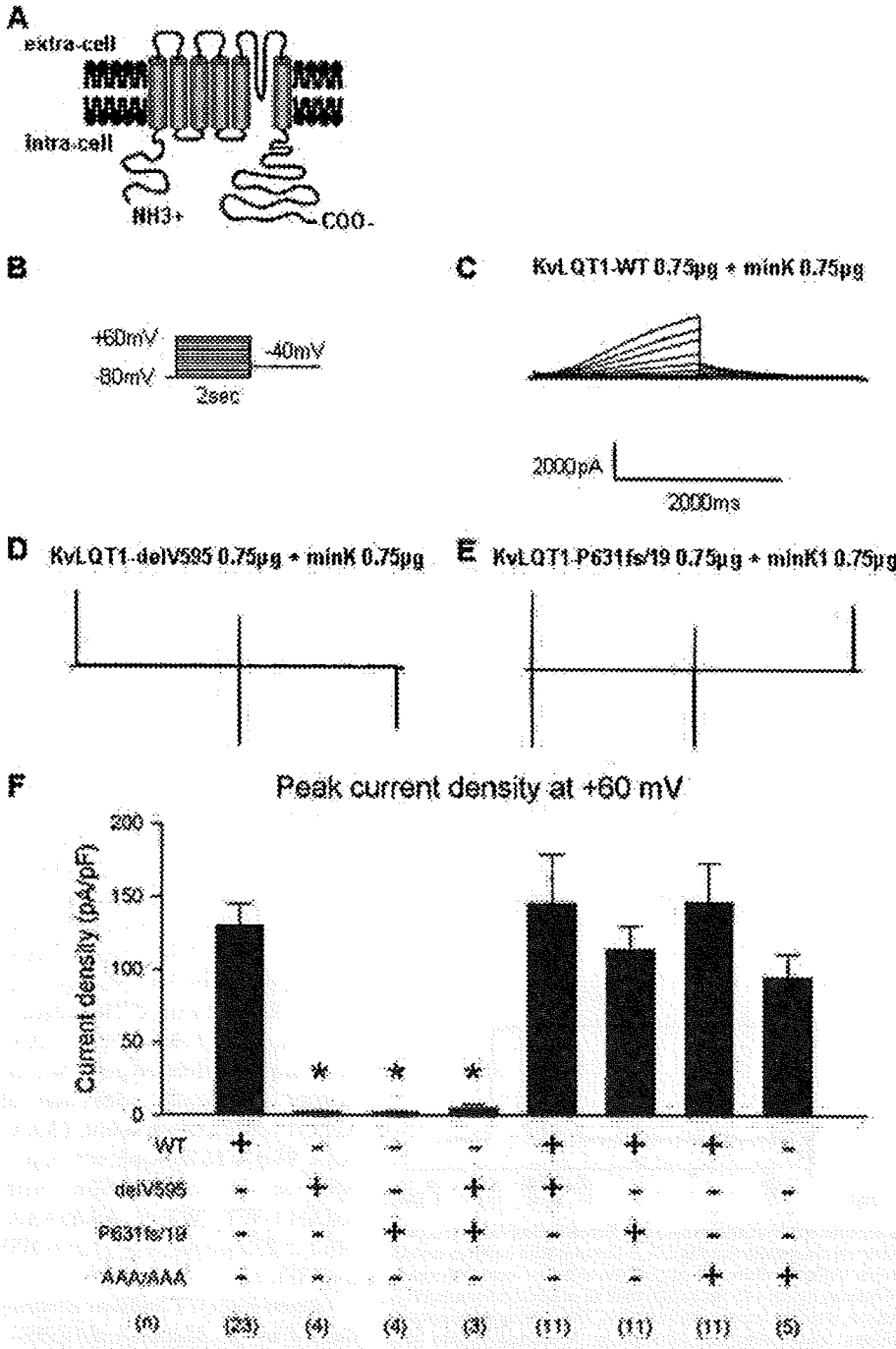

FIGURE 3. **Whole-cell patch clamp recording of the KvLQT1 channel.** *A*, schematic representation of full-length KvLQT1 channel analyzed in the electrophysiological study. *B*, the pulse protocol of whole-cell patch clamp recording from CHO-K1 cells transiently transfected with the EGFP-KvLQT1 plasmid (full-length KvLQT1-WT or -mutant) in combination with the CD8-MinK plasmid. *C–E*, representative current traces for KvLQT1-WT, -delV595, and -P631fs/19, respectively. *F*, *bar graph* representing the levels of peak current densities measured at the end of the 2-s test pulse at +60 mV. Combinations of KvLQT1-WT plasmid with KvLQT1-WT or -mutant plasmid for transfection are indicated *below*. AAA/AAA, the ER retention signal-deficient mutant (P631fs/19 carrying $A^{633}AA + A^{646}AA$). Data are represented as means ± S.E. *, $p < 0.0001$ *versus* WT. The number of experiments for each combination is indicated in *parentheses*.

cipitated by anti-GAL4 monoclonal antibody (Fig. 4, *B* and *C*). The binding of C terminus KvLQT1-delV595 with C terminus KvLQT1-WT, -P631fs/19, or -delV595 significantly decreased when compared with the binding that occurred between two C terminus KvLQT1-WTs (0.17 ± 0.03, 0.07 ± 0.02, or 0.19 ± 0.04 AU, respectively, $p < 0.001$ in each case). Although the binding of C terminus KvLQT1-R594Q with C terminus KvLQT1-WT increased significantly (2.09 ± 0.05 AU, $p < 0.001$), the binding of C terminus KvLQT1-P631fs/19 with C terminus KvLQT1-WT or -P631fs/19 showed virtually no change. These data indicated that the delV595 mutation impaired the subunit assembly.

Altered Localization of KvLQT1 Channel Caused by the Mutations—To investigate the functional consequence of the *KCNQ1* mutations further, we examined cell surface expression and cytoplasmic distribution of mutant KvLQT1 proteins. HEK293 cells transfected with L1-Myc-KvLQT1-WT, -delV595, or -P631fs/19 constructs (Fig. 5*A*) were immunostained using anti-c-Myc Ab under non-permeabilized or permeabilized conditions. Under non-permeabilized conditions in which α-tubulin was not detected (Fig. 5*B*, *a*), L1-Myc-KvLQT1-WT was expressed at the cell surface (Fig. 5*D*, *a*), but L1-Myc-KvLQT1-delV595 showed reduced cell surface expression (Fig. 5*D*, *b*). Under the permeabilized condition in which α-tubulin was detected (Fig. 5*B*, *b*), L1-Myc-KvLQT1-delV595 represented an abnormal intracellular granular pattern with reduced fluorescence intensity (Fig. 5*D*, *e* and *g*), whereas a diffuse reticular pattern was found for L1-Myc-KvLQT1-WT (Fig. 5*D*, *d*). L1-Myc-KvLQT1-P631fs/19 showed abnormal localization similar to that of L1-Myc-KvLQT1-delV595 (Fig. 5*D*, *c*, *f*, and *h*). The abnormal localizations caused by the mutations were not suppressed by the presence of MinK, which had a critical chaperone-like function (Fig. 5*E*). To corroborate the reduced cell surface expression of KvLQT1-delV595 and -P631fs/19, Western blot analysis was performed for the membrane protein-enriched fraction from cells transfected with Nt-Myc-KvLQT1 constructs (schematic representation is shown in Fig. 6*A*). It was demonstrated that the expression of the KvLQT1 channel in the membrane fraction was significantly decreased

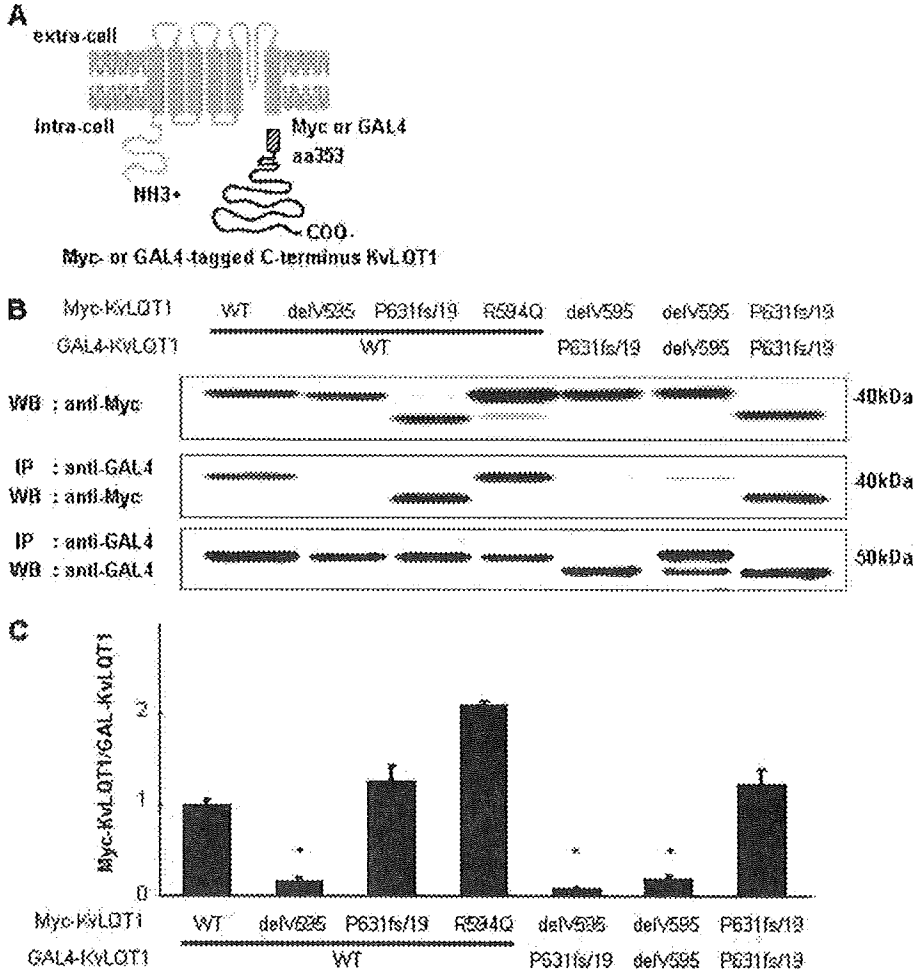

FIGURE 4. **Binding of C terminus KvLQT1 proteins.** *A*, schematic representation of constructs used in this experiment. C-terminal cytoplasmic domain of KvLQT1 protein was tagged with Myc or GAL4. *B* (*top*), amounts of Myc-tagged C terminus KvLQT1 expressed in transfected COS-7 cells as measured by Western blot analysis of whole-cell supernatants. *Middle*, amount of Myc-tagged C terminus KvLQT1 after co-IP with GAL4-tagged C terminus KvLQT1. *Bottom*, amounts of GAL4-tagged C terminus KvLQT1 after the co-IP with GAL4-tagged C terminus KvLQT1. *C*, ratios of the amount of Myc-tagged C terminus KvLQT1 to that of GAL4-tagged C terminus KvLQT1 after the co-IP. Densitometric data for Myc-tagged C terminus KvLQT1-WT and GAL4-tagged C terminus KvLQT1-WT were arbitrarily defined as 1.0. Data are represented as means ± S.E. ($n = 4$ for each case). *, $p < 0.001$ *versus* WT.

by the delV595 and P631fs/19 mutations (0.49 ± 0.06 and 0.09 ± 0.06 AU, respectively, $p < 0.001$ in each case), although a similar amount of caveolin-1, a marker of the membrane proteins, was detected in the analyzed fractions (Fig. 5*F*). Because the reduced expression level of full-length KvLQT1 in the membrane fraction might be specific to the Myc-tagged KvLQT1, we examined the expression of mutant KvLQT1 proteins in cells transfected with the GFP-tagged full-length KvLQT1 constructs and found again the decreased expression of KvLQT1 carrying each mutation (data not shown).

Altered Stabilization and Subcellular Fraction of KvLQT1 Channel Caused by the Mutations—To investigate further the expressivity and stability of mutant KvLQT1 proteins, we examined the expression of Nt-Myc-KvLQT1-WT, -delV595, and -P631fs/19 proteins (Fig. 6*A*) in the cells co-transfected with Myc-tagged C terminus KvLQT1-WT, -delV595, and -P631fs/19 (Fig. 4*A*), respectively. Western blot analyses of total cellular proteins at 12, 24, 48, and 72 h after transfection in HEK293 cells demonstrated that both Nt-Myc-KvLQT1-delV595 and -P631fs/19 mutant proteins expressed statistically lower than the Nt-Myc-KvLQT1-WT protein, whereas the Myc-tagged C terminus KvLQT1 proteins expressed at similar levels (Fig. 6, *B* and *C*). In addition, the amount of mutant proteins decreased, especially at 72 h, suggesting that both mutations affected the stability of KvLQT1.

Abnormal Cytoplasmic Localization of Mutant KvLQT1—To examine the intracellular distribution of the mutant KvLQT1 proteins, cells transfected with L1-Myc-KvLQT1 constructs were co-immunostained for c-Myc and calnexin (a marker for ER) under the permeabilized conditions. Cytoplasmic reticular distribution of L1-Myc-KvLQT1-WT was found with calnexin (Fig. 7*A*, *a–c*). On the other hand, L1-Myc-KvLQT1-delV595 and -P631fs/19 showed reticular and abnormal intracellular granular patterns with aggregates, and these aggregates were at least in part co-localized with calnexin (Fig. 7*A*, *d–f* and *g–i*, respectively). These data suggested that both L1-Myc-KvLQT1-delV595 and -P631fs/19 were localized to the ER and adjacent organelle, presumably the Golgi apparatus. In addition, we examined the cellular distribution of Myc-tagged C terminus KvLQT1. It was found that both normal and mutant C terminus KvLQT1 proteins did not express on the cell surface and showed a diffuse intracellular distribution pattern (Fig. 7*B*).

To investigate the cause of the trafficking defect due to the P631fs/19 mutation, we made two additional constructs (Fig. 8*A*). One was P631stop, in which the 19 amino acids generated by the frameshift were removed, and the other was an artificial frameshift derived from the insertion of two nucleotides, resulting in the addition of 34 amino acids (P631fs2/34). To our surprise, both L1-Myc-KvLQT1-P631stop and -P631fs2/34 were expressed well at the cell surface under the non-permeabilized condition (Fig. 8*B*, *a* and *b*, respectively). Furthermore, these KvLQT1 proteins showed cytoplasmic reticular distribution patterns under the permeabilized condition (Fig. 8*B*, *f* and *g*, respectively), indicating that the 19 residues in P631fs/19 caused the intracellular aggregation and trafficking defect. We hypothesized that there might be a retention signal to ER and/or Golgi in the 19 residues that caused the trafficking